

1 **Air temperature variability over three glaciers in the Ortles-Cevedale (Italian**  
2 **Alps): effects of glacier fragmentation, comparison of calculation methods and**  
3 **impacts on mass balance modeling**

4  
5 Luca Carturan<sup>1</sup>, Federico Cazorzi<sup>2</sup>, Fabrizio De Blasi<sup>1</sup>, Giancarlo Dalla Fontana<sup>1</sup>

6 <sup>1</sup> Department of Land, Environment, Agriculture and Forestry, University of Padova, Viale  
7 dell'Università 16 - 35020 - Legnaro, Padova, Italy

8 <sup>2</sup> Department of Agriculture and Environmental Sciences, University of Udine, via delle Scienze  
9 208 - 33100 - Udine, Italy

10  
11 Corresponding author: [luca.carturan@unipd.it](mailto:luca.carturan@unipd.it)  
12

13  
14 **Abstract**

15 Glacier mass balance models rely on accurate spatial calculation of input data, in particular air  
16 temperature. Lower temperatures (the so-called glacier cooling effect), and lower temperature  
17 variability (the so-called glacier damping effect) generally occur over glaciers, compared to ambient  
18 conditions. These effects, which depend on the geometric characteristics of glaciers and display a  
19 high spatial and temporal variability, have been mostly investigated on medium- to large-size  
20 glaciers so far, while observations on smaller ice bodies ( $< 0.5 \text{ km}^2$ ) are scarce. Using a dataset  
21 from 8 on-glacier and 4 off-glacier weather stations, collected in summer 2010 and 2011, we  
22 analyzed the air temperature variability and wind regime over three different glaciers in the Ortles-  
23 Cevedale. The magnitude of the cooling effect and the occurrence of katabatic boundary layer  
24 (KBL) processes showed remarkable differences among the three ice bodies, suggesting the likely  
25 existence of important reinforcing mechanisms during glacier decay and fragmentation. The  
26 methods proposed by Greuell and Böhm (1998) and Shea and Moore (2010) for calculating on-  
27 glacier temperature from off-glacier data did not fully reproduce our observations. Among them, the  
28 more physically-based procedure of Greuell and Böhm (1998) provided the best overall results  
29 where the KBL prevails, but it was not effective elsewhere (i.e. on smaller ice bodies and close to  
30 the glacier margins). The accuracy of air temperature estimations strongly impacted the results from  
31 a mass balance model which was applied to the three investigated glaciers. Most importantly, even  
32 small temperature deviations caused distortions in parameter calibration, thus compromising the  
33 model generalizability.

## 34 **1 Introduction and background**

35 Air temperature exerts a crucial control on the energy and mass exchanges occurring at the glacier  
36 surface. It regulates the accumulation processes via the snowfall elevation limit and the snowpack  
37 metamorphism (which affect redistribution phenomena), and regulates the ablation processes via  
38 turbulent fluxes and longwave radiation. It is also closely related to important feedbacks such as  
39 albedo, the mass balance–elevation feedback, and the glacier cooling effect, which changes as  
40 glaciers adjust their size in response to climatic fluctuations (Khodakov, 1975; Klok and Oerlemans,  
41 2004; Paul et al., 2005; Raymond and Neumann, 2005; Haeberli et al., 2007; Fischer, 2010; Paul,  
42 2010; Carturan et al., 2013).

43 Distributed models of different complexity have been proposed for calculating the mass balance of  
44 glaciers under different climatic scenarios at a variety of spatial scales and with different purposes.  
45 The current concern about sea level rise and future availability of water resources stored in glaciers,  
46 under projected global warming scenarios, has led to increased efforts to develop models able to  
47 account for i) direct effects of climate change, and ii) reinforcing mechanisms which control glacier  
48 decay (Hock, 2005; Barry, 2006).

49 These models rely on accurate spatial calculation of input data, in particular air temperature, which  
50 affects not only their final performance but also the calibration of parameters and model  
51 generalizability. Indeed, wrong temperature estimates lead to wrong calibration and/or distortion of  
52 parameters, possibly hampering the applicability of models to ungauged catchments, despite the  
53 good knowledge achieved for individual processes (Savenije, 2001; Sivapalan, 2006).

54 Charbonneau et al. (1981), for example, highlighted that issues in extrapolating meteorological  
55 input data are much more crucial than the possible choice between different approaches for  
56 modeling snow yields from a well-equipped catchment in the French Alps. Similarly,  
57 intercomparison projects of runoff models by the World Meteorological Organization (e.g. WMO,  
58 1986) revealed that simple models provided comparable results to more sophisticated models, given  
59 the difficulties of assigning proper model parameters and meteorological input data to each  
60 catchment element. Machguth et al. (2008), analyzing model uncertainty with Monte Carlo  
61 simulations at one point on the tongue of Morteratsch Glacier in Switzerland, concluded that the  
62 output of well-calibrated models, when applied to extrapolate in time and space, is subject to  
63 considerable uncertainties due to the quality of input data. According to Carturan et al. (2012a),  
64 who compared three melt algorithms in a six-year application of an enhanced temperature-index  
65 model over two Italian glaciers, uncertainties in extrapolating temperature measurements from off-  
66 site data partly mask the peculiar behavior of each algorithm and do not allow definitive  
67 conclusions to be drawn.

68 Two main issues affect the correct estimation of air temperature distribution over glacial surfaces: i)  
69 the absence of on-site weather stations in most operational model applications, and ii) the  
70 development of a katabatic boundary layer (KBL) over the typically inclined glacier surfaces (van  
71 den Broeke, 1997). Several experiments with automatic weather stations deployed over glaciers  
72 demonstrated that general assumptions in extrapolating air temperature, based on the application of  
73 fixed lapse rates which account for the linear dependency of ambient (i.e. off-glacier) temperature  
74 on altitude, have serious limitations (e.g. Greuell et al., 1997; Strasser et al., 2004; Petersen and  
75 Pellicciotti, 2011).

76 In particular, these assumptions do not apply when katabatic flows and the KBL form, that is,  
77 during the ablation season on melting mid-latitude glacial surfaces, when the ambient temperature is  
78 higher than the surface temperature which cannot exceed 0°C. Katabatic winds are gravity winds  
79 originated by the cooling of the near-surface air layers, resulting in density gradients which force a  
80 downward movement of the air under the effect of gravity. The two main processes affecting the

81 temperature of the air during this downslope movement are the cooling due to the exchange of  
82 sensible heat and the adiabatic heating. The interplay of these processes has a twofold effect,  
83 consisting in lower on-glacier temperatures (the so-called glacier cooling effect), and lower  
84 temperature variability (the so-called glacier damping effect, also referred to as reduced climate  
85 sensitivity), compared to ambient conditions (Braithwaite, 1980; Greuell and Böhm, 1998;  
86 Braithwaite et al., 2002; Gardner et al., 2009). As a result, on-glacier lapse rates generally differ  
87 from average environmental lapse rates (i.e.  $-0.0065^{\circ}\text{C m}^{-1}$ ). Cooling and damping effects are not  
88 homogeneous over glacial surfaces, and mainly depend on the size and geometric characteristics, in  
89 particular the slope, of single glaciers, and on the specific position along the glacier. Generally, they  
90 are directly related to the size of glaciers and the fetch distance along the flowline, and inversely  
91 related to the slope of glaciers. The latest controls the prevalence of the cooling due to turbulent  
92 exchanges over the adiabatic heating of air forced to move downward by katabatic winds.

93 Few methods have been proposed in the literature to model these processes, mainly due to the  
94 scarcity of glaciers instrumented for distributed measurements of air temperature. Among the first  
95 authors who measured the glacier cooling effect, defined as the temperature difference between an  
96 on-glacier and an off-glacier site with the same altitude, we can cite Schytt (1955) and Eriksson  
97 (1958), who detected temperature depressions ranging from 1.1 to 2.2°C on Storglaciären (Sweden)  
98 and 3 to 4°C on Skagastøl Glacier (Norway), respectively. Havens (1964) measured an average  
99 cooling effect ranging from 1.5°C to 2.7°C at a weather station located 1 km up-glacier from the  
100 terminus of White Glacier (Canada), recognizing maximum values during warm and sunny weather  
101 and minimum values during overcast and unsettled weather.

102 To our knowledge, the first attempt to parameterize the mean summer cooling effect at the firn line  
103 altitude was made by Khodakov (1975), who proposed a relationship with glacier length, based on  
104 temperature data obtained from mountain glaciers and ice sheets. Analyzing direct observations  
105 from glaciers in Caucasus, Pamir, Scandinavia, Thien Shan, and Altay, Davidovich and Ananicheva  
106 (1996) provided a simple relationship for calculating the mean summer temperature at the  
107 equilibrium line altitude (ELA) in function of the mean off-glacier summer temperature at the same  
108 altitude. The same authors suggested that the cooling effect is maximal at the ELA and decreases  
109 towards both the terminus and up-glacier.

110 The first comprehensive glacio-meteorological experiment providing distributed temperature  
111 measurements was carried out in summer 1994 on Pasterze Glacier, Austria, and comprised five  
112 automatic weather stations (AWS) placed along a flowline. From this experiment, Greuell and  
113 Böhm (1998) developed a thermodynamic model for calculating air temperature in function of slope  
114 and distance along the flowline, accounting for sensible heat exchanges and adiabatic heating.  
115 Braithwaite et al. (2002) used an empirical approach and a formulation derived from data gathered  
116 in two Canadian Arctic glaciers (Sverdrup and White), similar to that proposed by Davidovich and  
117 Ananicheva (1996) but applied to monthly temperatures. Shea and Moore (2010) suggested  
118 empirical relationships based on piecewise linear regressions of on-glacier versus ambient  
119 temperatures collected in British Columbia (Canada) between 2006 and 2008, for calculating i) the  
120 threshold temperature triggering KBL development, and ii) the glacier damping effect, as a function  
121 of elevation and flow path length (i.e. the 'average flow distance to a given point starting from an  
122 upslope limit or ridge').

123 At present these methods have rarely been used by other authors, and they have not been compared  
124 using independent test sites. Petersen et al. (2013) tested the Greuell and Böhm (1998) model using  
125 a dataset of air temperature measurements from Haut Glacier d'Arolla, Switzerland, concluding that  
126 results of spatial extrapolations along the glacier are only a little better than using a constant linear  
127 lapse rate calculated between on-glacier data points, attributing this result to the spatial variability  
128 of the thickness of the glacier boundary layer.

129 The transferability of the proposed methods remains to be tested. In addition, it should be noted that  
130 many of them have been developed using temperature data collected from medium- (from 0.5 to 10  
131 km<sup>2</sup>) to large-sized (larger than 10 km<sup>2</sup>) glaciers. As the glacier cooling effect and the damping  
132 effect depend on the size of glaciers, it is opportune to investigate the thermal effects of ice bodies  
133 smaller than 0.5 km<sup>2</sup>, which are widespread and increasing in number in mid-latitude mountain  
134 regions as a result of rapid shrinking and fragmentation.

135 In this work we present the results of a glacio-meteorological experiment, carried out in summer  
136 2010 and 2011, deploying several automatic weather stations over three neighboring glaciers in the  
137 Ortles-Cevedale mountain group (Italian Alps). The study was focused on the variability of air  
138 temperature over the three glaciers, which differ in size, geometric characteristics, and reaction to  
139 climatic changes (Carturan et al., 2014). In this paper, we analyze the temporal and spatial behavior  
140 of air temperature and glacier cooling effect in the study area, testing existing methods for  
141 calculating on-glacier temperatures from off-site data, and evaluating their impact in mass balance  
142 simulations using a distributed enhanced temperature-index (ETI) model.

143

## 144 **2 Study area**

145 The investigated glaciers are located in the Alta Val de la Mare (AVDM), Eastern Italian Alps (Fig.  
146 1). This 36 km<sup>2</sup> experimental watershed is the subject of detailed studies concerning the impacts of  
147 climate change on the cryosphere and hydrology. The area has previously been selected for  
148 studying the behavior of meteorological variables at high altitude (Carturan et al., 2012b) and for  
149 developing an enhanced temperature-index glacier mass balance model (Carturan et al., 2012a). The  
150 highest summit is Mt Cevedale (3769 m a.s.l.), while the basin outlet is located at 1950 m a.s.l. The  
151 catchment lies in the southern part of the Ortles-Cevedale massif, the largest glacierized mountain  
152 group in the Italian Alps. The Careser diga weather station (2607 m a.s.l.) has been operating since  
153 the 1930s, recording daily 2 m air temperature, precipitation, snow depth, and fresh-snow height. In  
154 the 1990s, an automatic weather station replaced the old manual instruments. At this site, the mean  
155 1979–2009 annual precipitation (corrected for gauge errors) was 1233 mm and the mean annual air  
156 temperature in the same period was –0.5 °C.

157 The investigated glaciers are very different. Careser Glacier (2870– 3279 m a.s.l.) is flat and mainly  
158 exposed to the south. In 2005 it spread in two parts: Careser Orientale (2.13 km<sup>2</sup> in 2006) and  
159 Careser Occidentale (0.27 km<sup>2</sup> in 2006). La Mare Glacier (2650–3769 m a.s.l., 3.79 km<sup>2</sup> in 2006)  
160 faces to the east and is steeper. On all glaciers, topographic shading is of minor importance. The  
161 Careser glaciers have no accumulation area and exhibit down-wasting and fragmentation in smaller  
162 units (Carturan et al., 2013), while La Mare Glacier still has an accumulation area and shows ‘active’  
163 retreat towards higher altitudes (Zanon, 1982; Small, 1995; Carturan et al., 2009 and 2014). Long-  
164 term monitoring programs started in 1967 on Careser and in 2003 on La Mare. In the last 10 years,  
165 the glaciers have been the subject of investigations on snow accumulation, snow and ice ablation,  
166 point energy balance, and runoff generation (Carturan, 2010).

167

## 168 **3 Methods**

### 169 **3.1 Experimental setup**

170 An automatic weather station (AWS) has been operating since July 2007 on the ablation area of La  
171 Mare Glacier (2973 m a.s.l.), measuring air temperature and relative humidity, wind speed and  
172 direction, incoming and outgoing shortwave and longwave radiation, and snow depth. The thermo-

173 hygrometric probe is housed in a ventilated radiation shield. Data are sampled every 60 seconds,  
174 with 15 minute means being stored in a Campbell Scientific CR1000 datalogger; the AWS is  
175 powered by a 25 W solar panel. Data were periodically downloaded with a portable laptop until  
176 July 2011. Since August 2011, a satellite modem has automatically transmitted data at three-day  
177 intervals (Abbate et al., 2013).

178 On 3 July 2010 three Vantage Pro Plus (VPP) weather stations, manufactured by Davis Instruments,  
179 were placed along a longitudinal profile on La Mare Glacier at elevations ranging from 2709 m,  
180 close to the terminus, to 3438 m, near to the upper divide. Davis VPP stations are low-cost,  
181 commercial weather stations, characterized by a compact design and low weight, and can be moved  
182 rather easily along glaciers by few persons. Their thermo-hygrometric probe is shielded by a  
183 ventilated screen, which is important for air temperature measurements in high-radiation and/or  
184 low-wind speed conditions on glaciers (Georges and Kaser, 2002). Hourly mean data are stored in a  
185 Davis datalogger. During the experiment, the data were downloaded with a portable laptop every  
186 two weeks. The three VPP were removed on 23 September 2010.

187 On 7 July 2011 four VPP stations were deployed, two on Careser Glacier and two on La Mare  
188 Glacier. One weather station was re-positioned at 3438 m on La Mare Glacier because  
189 instrumentation failure occurred at that place in 2010, due to lightning damage. The other three  
190 weather stations were placed in areas where systematic errors in mass balance simulations were  
191 recognized by Carturan et al. (2012a), who applied a mass balance model using the standard  
192 environmental lapse rate for extrapolating air temperature from an off-glacier weather station, as  
193 commonly used in most model applications where on-glacier data are not available. The four VPP  
194 were removed on 12 September 2011.

195 Table 1 reports the configuration of the weather stations operated on Careser and La Mare glaciers,  
196 whose location is shown in Fig. 1. Four off-glacier weather stations (Table 1) were also used in this  
197 study for the calculation of the glacier cooling effect in comparison to ambient temperature, and for  
198 testing two methods of calculation of on-glacier temperatures from off-site data. Two of them are  
199 part of the regional weather station networks (Bel\_3328, at Cima Beltovo, 3328 m a.s.l.; Cog\_1202,  
200 at Cogolo Pont, 1202 m a.s.l., Fig. 1). The other two weather stations consist of Hobo Pro  
201 dataloggers (Onset Computer Corporation) installed at Careser diga (Car\_2607, at 2607 m a.s.l.)  
202 and close to Careser Glacier (Car\_3051, at 3051 m a.s.l.). All these stations are far enough from the  
203 thermal influence of glaciers (minimum distance of 300 m from Car\_3051 to the margin of Careser  
204 Glacier), and equipped with temperature probes housed in naturally ventilated radiation shields.  
205 Possible issues related to the use of different types of temperature sensors and radiation shields are  
206 addressed in the following section.

### 207 **3.2 Data processing and accuracy assessment**

208 For our analyses, hourly means were calculated from sub-hourly meteorological data. After being  
209 synchronized with local solar time, the data were checked for possible gaps, outliers, and  
210 inhomogeneities. The major gap concerned a few days in summer 2011 for the precipitation data at  
211 Careser diga, which were filled using the manual observations recorded by the personnel of the  
212 local hydropower company. Other gaps of 1-2 hours occurred during the maintenance of weather  
213 stations, and were filled by linear interpolation.

214 The spatial density and type of weather stations used in this study were decided based on i) the pre-  
215 existing network of regional AWSs and ii) the logistic constraints affecting the access to the  
216 glaciers and limiting the number of research-grade AWSs which could be deployed. These  
217 limitations are common in mountain regions, and imposed comparable or even lower densities of  
218 AWSs, as well as the use of different types of sensors with different radiation shields, in most

219 similar studies on glaciers (e.g. Shea and Moore, 2010; Petersen and Pellicciotti, 2011; Petersen et  
220 al., 2013).

221 Intercomparison tests have been carried out in order to assess the impact of using different sensors  
222 and radiation shields for this study. The four VPP weather stations were run for some days within a  
223 10-m radius, both before and after the glacio-meteorological experiment, confirming the almost  
224 identical readings of air temperature, wind speed, and wind direction. Mean differences in air  
225 temperature data during the tests were lower than 0.20°C (maximum STD = 0.16°C). For  
226 comparison purposes, one VPP was run close to the AWS of La Mare Glacier in summer 2009,  
227 revealing mean differences in air temperature readings of 0.10°C (STD = 0.12°C). A further  
228 comparison was carried out in the summers of 2007 and 2008, running a VPP close to the Hobo Pro  
229 datalogger and close to a temperature sensor of the regional weather service installed at Careser  
230 diga. These two instruments, which have natural ventilation systems, showed mean differences of  
231 0.10°C (STD = 0.40°C) and 0.23°C (STD = 0.66°C), respectively, compared to the aspirated VPP.  
232 Based on these results, no corrections were applied to the measured air temperatures.

### 233 3.3 Analysis of field data

234 The meteorological data collected by the weather stations were firstly analyzed calculating  
235 descriptive statistics for each of the two summers 2010 and 2011 and focusing on vertical lapse  
236 rates. Afterwards, the data were analyzed at hourly resolution focusing on the calculation of  
237 ambient (i.e. off-glacier) temperature, which is crucial for estimating on-glacier near-surface  
238 temperatures, and is required by all methods proposed in the literature for this purpose. Moreover,  
239 the correct estimation of the ambient temperature is an essential prerequisite for quantifying the  
240 site-specific cooling effect on glaciers, which is defined as 'the difference between screen-level  
241 temperatures over glaciers compared to equivalent-altitude temperatures in the free atmosphere'  
242 (Braithwaite, 1980). Different combinations of lapse rates (i.e. fixed standard or hourly-variable  
243 obtained by linear regression of temperature versus elevation) and subsets of weather stations were  
244 tested (see details in Sect. 4.2).

245 The spatial and temporal variability of the cooling effect was then investigated, plotting the average  
246 diurnal cycle of the cooling effect versus average cycles of wind speed and direction, and drawing  
247 charts of the daily average cooling effect vs. daily temperature and precipitation recorded at Careser  
248 diga, in order to assess the role of different weather types in the glacial temperature regimes.

### 249 3.4 Calculation of on-glacier temperature from off-site data

250 The measured on-glacier temperatures served for testing the procedures suggested by Shea and  
251 Moore (2010) and Greuell and Böhm (1998) (from now on “S&M” and “G&B”, respectively) for  
252 calculating the air temperature distribution over glacierized surfaces. The empirical methods by  
253 Khodakov (1975), Davidovich and Ananicheva (1996), and Braithwaite et al. (2002) were not tested  
254 because they are more empirical, the coefficients were calculated in very different environments,  
255 and they do not take into account the temporal variability of the cooling effect.

256 S&M suggested the use of a piecewise regression model:

$$257 T_g(x, t) = \begin{cases} T_1 + k_2(T_a - T^*), & T_a \geq T^* \\ T_1 - k_1(T^* - T_a), & T_a < T^* \end{cases} \quad (1)$$

258 where  $T_g(x, t)$  (°C) is the on-glacier temperature for site  $x$  at time  $t$ ,  $T^*$  (°C) represents a threshold  
259 ambient temperature for KBL effects on  $T_g$ ,  $T_l$  (°C) is the corresponding on-glacier threshold  
260 temperature,  $k_2$  ( $k_l$ ) is the so called sensitivity of on-glacier temperature to ambient temperature ( $T_a$ ,  
261 °C) changes when  $T_a$  is above (below)  $T^*$ . Empirical transfer functions were obtained by S&M,

262 relating the fitted coefficients ( $T^*$ ,  $k_1$  and  $k_2$ ) for each weather station used in their work to  
 263 topographic attributes extracted from a digital elevation model (DEM):

$$264 \quad T^* = \beta_1 + \beta_2 Z \quad (2)$$

$$265 \quad k_1 = \beta_3 \exp(\beta_4 FPL) \quad (3)$$

$$266 \quad k_2 = \beta_5 + \beta_6 \exp(\beta_7 FPL) \quad (4)$$

267 where  $\beta_i$  are the coefficients of the transfer functions,  $Z$  (m) is the elevation, and  $FPL$  (m) is the  
 268 flow path length, defined as ‘the average flow distance to a given point starting from an upslope  
 269 summit or ridge’ (Shea and Moore, 2010).  $T_I$  is calculated as  $T^* \cdot k_I$ .

270 The G&B model assumes the presence of a katabatic wind, and therefore it applies when the  
 271 ambient temperature is higher than the surface temperature. In these conditions the potential  
 272 temperature  $\theta$  ( $^{\circ}\text{C}$ ) at the distance  $x$  along the flowline ( $x = 0$  at the top of the flowline) is calculated  
 273 as:

$$274 \quad \theta(x) = (T_0 - T_{eq}) \exp\left(-\frac{x-x_0}{L_R}\right) - b(x + x_0) + T_{eq} \quad (5)$$

275 with

$$276 \quad T_0 = T_{cs} - \gamma(z_{cs} - z_0) \quad (6)$$

$$277 \quad T_{eq} = bL_R \quad (7)$$

$$278 \quad L_R = \frac{H \cos(\alpha)}{C_H} \quad (8)$$

$$279 \quad b = \Gamma_d \tan(\alpha) \quad (9)$$

280 where  $T_0$  ( $^{\circ}\text{C}$ ) is the temperature at  $x = 0$ ,  $T_{eq}$  ( $^{\circ}\text{C}$ ) is defined as the ‘equilibrium temperature’,  $x_0$   
 281 and  $z_0$  (m) are the location and elevation where the air enters the glacier-wind layer,  $T_{cs}$  ( $^{\circ}\text{C}$ ) and  $z_{cs}$   
 282 (m) are the temperature and the elevation at the off-glacier weather station,  $\gamma$  ( $^{\circ}\text{C m}^{-1}$ ) is the ambient  
 283 lapse rate,  $H$  (m) is the height of the glacier wind layer,  $\alpha$  ( $^{\circ}$ ) is the glacier slope,  $C_H$  is the bulk  
 284 transfer coefficient for heat, and  $\Gamma_d$  is the dry adiabatic lapse rate ( $-0.0098^{\circ}\text{C m}^{-1}$ ). The potential  
 285 temperature is converted into temperature by means of:

$$286 \quad T(x, z) = \theta(x) - \Gamma_d [z(x = 0) - z(x)] \quad (10)$$

287 where  $z(x)$  is the surface profile of the glacier.

288 For both methods, the original formulations and parameters were tested unchanged against our  
 289 experimental data, evaluating also possible modifications as detailed in Sect. 4. The efficiency was  
 290 evaluated by means of three different statistics: i) the mean error (ME), ii) the root mean square  
 291 error (RMSE), and iii) the efficiency criterion by Nash and Sutcliffe (N&S, 1970). The topographic  
 292 information required to apply these methods was extracted from a 2 x 2 m DEM surveyed by  
 293 LiDAR in late summer of 2006. A map of the FPL was calculated from this DEM, using algorithms  
 294 developed for drainage area calculations (Fig. 2, Tarboton et al., 1991).

### 295 **3.5 Mass balance modeling**

296 The impact that the calculation of on-glacier temperatures according to different methods has on  
 297 mass balance modelling was assessed using EISModel (Cazorzi and Dalla Fontana, 1996), which  
 298 was already applied to Careser and La Mare glaciers by Carturan et al. (2012a). EISModel employs

299 an enhanced temperature-index approach for computing melt, using the clear-sky shortwave  
300 radiation calculated from the DEM as a distributed morpho-energetic index. The model, which is  
301 suitable for applications on glaciers with limited data availability, doesn't require incoming  
302 shortwave radiation measurements, which are less commonly available compared to air temperature  
303 and precipitation.

304 Three melt algorithms (multiplicative, additive, and extended) have been implemented and can be  
305 used alternatively in EISModel. In the present work we use the additive melt algorithm, which  
306 explicitly separates the thermal and radiative components:

$$307 \quad MLT_{X,t} = [TMF \cdot T_{X,t}] + [RMF \cdot CSR_{X,t}(1 - \alpha_{X,t})] \quad (11)$$

308 where  $TMF$  and  $RMF$  are empirical coefficients called the Temperature Melt Factor ( $\text{mm h}^{-1} \text{ } ^\circ\text{C}^{-1}$ )  
309 and the Radiation Melt Factor ( $\text{mm h}^{-1} \text{W}^{-1} \text{ m}^2$ ),  $T_{X,t}$  ( $^\circ\text{C}$ ) is the air temperature at pixel  $X$  in hour  $t$ ,  
310  $CSR_{X,t}$  ( $\text{W m}^{-2}$ ) is the clear sky shortwave radiation and  $\alpha_{X,t}$  is the surface albedo (spatially variable  
311 for ice and spatially and temporally variable for snow). For a detailed description of the model we  
312 refer the reader to the work of Carturan et al. (2012a).

313 The cumulated mass balance measured at ablation stakes drilled in close proximity to the glacial  
314 weather stations (AWS and VPP) served for model calibration and validation. We used alternatively  
315 each of the two summer seasons of 2010 and 2011 as an independent dataset for  
316 calibration/validation. Point-based EISModel calculations at the weather stations were run, using  
317 four temperature series: i) measured data, ii) calculated temperature from Careser diga via the  
318 standard ambient lapse rate ( $-6.5^\circ\text{C km}^{-1}$ ), iii) calculated temperature according to the S&M  
319 method, and iv) calculated temperature according to the G&B method. Option ii) is commonly used  
320 in the absence of temperature data from glaciers (e.g. Gardner and Sharp, 2009; Michlmayr et al.,  
321 2008; Nolin et al., 2010).

322

## 323 **4 Results**

### 324 **4.1 Seasonal characteristics of temperature data**

325 A close dependency on altitude has been detected for mean summer air temperature, both outside  
326 the glaciers and, remarkably, over them (Table 2, Fig. 3). Because of thermal inversions occurring  
327 at the lowermost weather station (Cog\_1202) during the night and early morning, the vertical lapse  
328 rate was much steeper above Car\_2607 ( $-8.0^\circ\text{C km}^{-1}$  in 2010 and  $-8.3^\circ\text{C km}^{-1}$  in 2011) than below ( $-$   
329  $5.3^\circ\text{C km}^{-1}$  in 2010 and  $-5.2^\circ\text{C km}^{-1}$  in 2011). At a given altitude, the on-glacier air temperature was  
330 systematically lower than ambient temperature, the difference decreasing with altitude. Lapse rates  
331 were also lower on the glaciers ( $-7.2^\circ\text{C km}^{-1}$  in 2010 and  $-6.7^\circ\text{C km}^{-1}$  in 2011), compared to high-  
332 altitude off-glacier weather stations, and close to the standard ambient lapse rate ( $-6.5^\circ\text{C km}^{-1}$ ).  
333 Much shallower on-glacier lapse rates and fewer dependency of air temperature on elevation were  
334 found by earlier works (e.g. Greuell and Böhm, 1998; Strasser et al., 2004; Petersen et al. 2013). As  
335 reported in Table 2, the average daily temperature range and the average standard deviation are  
336 largest at the valley floor and both decrease with altitude, reaching their minima over the glaciers as  
337 previously reported, for example, by Oerlemans (2001). Hourly temperatures among different  
338 weather stations in Val de La Mare were highly correlated ( $r > 0.9$ , significant at the 0.001 level),  
339 with the remarkable exception of Cog\_1202, at the valley floor, whose correlation with the other  
340 weather stations ranged from 0.65 to 0.75, peaking at 0.84 with Car\_2607.

### 341 **4.2 Ambient temperature calculation**



342 For the calculation of ambient temperature at the altitude of glaciers, which is crucial for the  
343 quantification of the glacier cooling effect, we tested the following methods: i) use of a fixed  
344 standard ambient lapse rate ( $-6.5^{\circ}\text{C km}^{-1}$ ), ii) use of a fixed calibrated lapse rate (seasonal mean  
345 value), and iii) use of an hourly-variable lapse rate. Methods ii) and iii) were implemented using  
346 different combinations of off-glacier weather stations, calculating linear regressions of hourly  
347 temperature vs. altitude. The methods were tested removing alternatively Car\_3051 or Bel\_3328  
348 from linear regressions and using them for validation. The results, displayed in Table 3, show that  
349 regardless of the method used, the inclusion of the lowermost weather station gives poorer results.  
350 At Car\_3051, the method iii) applied to Car\_2607 and Bel\_3328 works best, indicating that in our  
351 case hourly variable lapse rates are the most appropriate solution while interpolating temperatures  
352 between two weather stations. Conversely, method ii) applied to Car\_2607 and Car\_3051 provides  
353 the best results at Bel\_3328, which suggests that a fixed calibrated lapse rate should be used while  
354 extrapolating above the uppermost station, even if uncertainty persists in these cases.

### 355 4.3 The glacier cooling effect

356 The cooling effect at each on-glacier weather station was calculated as the difference between the  
357 measured temperature and the ambient temperature at the same elevation, computed on the basis of  
358 the results described in Sect. 4.2 (i.e. hourly-variable lapse rate below Bel\_3328 and fixed  
359 calibrated lapse rate above it). The average seasonal cooling effect (Table 4) was maximal at Car-  
360 gl\_3082 ( $-1.01^{\circ}\text{C}$  in 2011) and at Mar-gl\_2973 ( $-0.74^{\circ}\text{C}$  in 2010 and  $-0.90^{\circ}\text{C}$  in 2011). Null or  
361 negligible cooling was detected at Mar-gl\_3438, close to the top of La Mare Glacier, and at Car-  
362 gl\_3144 on the small Careser Occidentale Glacier. Minor cooling occurred at Mar-gl\_3215 ( $-$   
363  $0.27^{\circ}\text{C}$  in 2010), which was close to the balanced-budget ELA of the glacier, and at Mar-gl\_3140 ( $-$   
364  $0.47^{\circ}\text{C}$  in 2011), in the upper ablation area. Notably, the narrow and steep terminus of La Mare  
365 Glacier experienced a significant cooling effect in 2010 ( $-0.65^{\circ}\text{C}$ ).

366 Fig. 4 reports the mean daily cycles of the cooling effect and wind regime. A common pattern  
367 emerges, with minimum cooling at night and maximum cooling around noon or in the afternoon,  
368 coherent with the diurnal cycle of ambient air temperature and deriving temperature differences  
369 from the glacier surface. For five out of the seven monitored sites, the cooling occurred almost  
370 exclusively during daytime. Nighttime cooling took place only at Mar-gl\_2973 and Car-gl\_3082,  
371 which are the two sites with higher mean cooling. Down-glacier winds dominated on La Mare  
372 Glacier, with higher speeds compared to Careser Occidentale and Orientale glaciers, where up-  
373 glacier winds prevailed. The wind speed was at its maximum at night on La Mare, especially in  
374 2010, while it was at its maximum in the afternoon on the two Careser glaciers. A peculiar behavior  
375 was found at the terminus of La Mare Glacier (Mar-gl\_2709), where down-glacier winds dominated  
376 at night, without a cooling effect, and were replaced by up-glacier winds from mid-morning to late  
377 afternoon, when the cooling effect increased sharply. Wind data were not available at Mar-gl\_3438,  
378 due to instrumentation failure, but we can argue that katabatic winds were not prevalent at this site,  
379 which is close to the crest, based on results published for similar locations in previous works (e.g.  
380 Greuell et al., 1997; Strasser et al., 2004).

381 Different weather conditions led to a considerable temporal variability of the glacier cooling effect  
382 during the two summer seasons of 2010 and 2011 (Fig. 5). Cooling was maximal during warm  
383 anticyclonic periods and nearly absent during cold unsettled weather. Differences among sites  
384 increased with warmer temperatures, whereas they nearly disappeared during cold and unstable  
385 periods. The highest variations occurred at Mar-gl\_2973, Mar-gl\_3215, Mar-gl\_3140, and Car-  
386 gl\_3082 while at Mar-gl\_3438 and Car-gl\_3144 there was a smaller temporal variability. A  
387 warming, rather than cooling, effect was observed on some days, mainly at the upper weather  
388 stations of La Mare Glacier. A close check on the wind and temperature data revealed that this was

389 ascribable to local föhn conditions, that is, forced adiabatic heating brought by strong northerly  
390 winds.

#### 391 4.4 Calculation of on-glacier temperature from off-site data

392 According to the S&M method, piecewise linear regressions of on-glacier hourly temperature  
393 versus ambient temperature at the same elevation have been calculated for each glacial weather  
394 station. The values of the parameters  $k_1$  and  $k_2$  (i.e. temperature sensitivities for ambient  
395 temperatures below and above the threshold temperature  $T^*$ , respectively) were well aligned with  
396 the transfer functions proposed by S&M, using the  $FPL$  as predictor (Fig. 6). On the other hand, the  
397 transfer function for  $T^*$  suggested by S&M, using station elevation as a predictor, could not be used  
398 in AVDM given the different geographic and climatic setting of the two study areas. We therefore  
399 propose to substitute Eq. (2) with the following function:

$$400 T^* = \frac{a \cdot FPL}{b + FPL} \quad (12)$$

401 which uses the  $FPL$  (m) rather than elevation as a predictor, thus being potentially more  
402 generalizable. The outlier already excluded by S&M was not included in our calculation of Eq. (12),  
403 nor was Mag-gl\_2709, both due to under-sampling at below-zero temperatures. Fig. 6 shows data  
404 points, transfer functions, and parameters. Calculated versus measured temperature is shown in Fig.  
405 7 along with related statistics. Four out of the five sites where the method works satisfactorily ( $ME$   
406  $< 0.5^\circ\text{C}$  in absolute value and  $N\&S$  index  $> 0.87$ ) have prevailing katabatic winds. On the contrary,  
407 lower performance affects sites close to the glacier margin (Mar-gl\_3438 and, in particular, Mar-  
408 gl\_2709), where katabatic winds are disrupted by valley winds or synoptic winds, and Car-gl\_3082,  
409 where up-glacier winds prevail. The efficiency statistics for all sites are:  $ME = -0.06^\circ\text{C}$ ,  $RMSE =$   
410  $0.73^\circ\text{C}$  and  $N\&S = 0.692$ .

411 According to the G&B method, the location  $x_0$  where the air enters the glacier wind layer, and the  
412 length scale  $L_R$ , can be calculated by an exponential function which expresses the 'climatic  
413 sensitivity' in function of the distance  $x$  along the flowline:

$$414 \frac{dT(x)}{dT_{cs}} = \exp\left(-\frac{x+x_0}{L_R}\right) \quad (13)$$

415 Climatic sensitivities were calculated, comparing daily mean temperature at our on-glacier sites to  
416 daily mean temperature at Car\_3051, and have been added for comparison to the data displayed in  
417 Figure 5 of the Greuell and Böhm (1998) paper. The results are shown in Fig. 8 and indicate a fairly  
418 good alignment of our data with the other glaciers' data and with the best fit calculated by G&B for  
419 the Pasterze weather stations. It therefore seemed appropriate to use the values of  $x_0$  and  $L_R$   
420 calculated by those authors, that is, 1440 and 8340 m respectively. According to the G&B  
421 procedure, the hourly temperature above the freezing level was set equal to the ambient temperature  
422 (Sect. 4.2). Below the freezing level, the glacier-wind model of G&B was applied, setting i)  $x_0 = 0$   
423 if the freezing level was below the top of the flowline, and ii)  $x_0 = 1440$  m if it was above this point,  
424 in order to take into account a climate sensitivity  $< 1$  at the top of the flowline.  $z_0$  was set equal to  
425 the freezing level in case i) and equal to the altitude of the top of the flowline in case ii). These  
426 settings are the same as those used in the G&B paper. Nevertheless, no corrections were applied to  
427 the computed temperatures, as was done by G&B, who applied a fixed offset of  $-0.74^\circ\text{C}$ .

428 Fig. 9 displays the results of the G&B method. Calculated temperatures matched the measured  
429 temperatures fairly well and the efficiency statistics for all sites were better than for the S&M  
430 method:  $ME = -0.27^\circ\text{C}$ ,  $RMSE = 0.40^\circ\text{C}$ ,  $N\&S = 0.908$ . Improvements were observed, in particular,  
431 at Mar-gl\_2709, Car-gl\_3082, and Mar-gl\_3438, even if these sites lack predominant katabatic  
432 winds. A clear step is observable at Mar-gl\_2709 and, slightly less obvious, at Mar-gl\_2973 in both

433 summer 2010 and 2011, attributable to the jump of  $x_0$  from 0 to 1440 m when the freezing level  
434 exceeds the top of the flowline.

435

#### 436 **4.5 Mass balance modeling**

437 EISModel applications using measured temperature datasets resulted in RMSE values well below  
438 the mass balance measurement error from ablation stakes readings (~200 mm w.e., Thibert et al.,  
439 2008; Huss et al., 2009), thus confirming the good skill of the modeling tool. On the other hand, the  
440 RMSE was nearly double when calculated temperature datasets were used as input, and  
441 considerable differences also exist in the calibration parameters (Table 5).

442 The spatial distribution of modeling errors using temperature extrapolations from Car\_2607 via the  
443 standard lapse rate (Fig. 10, scatterplots b1 to b4) replicated the findings of Carturan et al. (2012a)  
444 for the six previous years (2004 to 2009). In particular, the modeled vertical gradient of mass  
445 balance on La Mare Glacier in summer 2010 was lower than the observed one, in both calibration  
446 and validation runs, due to uneven errors in estimating air temperature (+0.77, +1.17, and +1.14°C  
447 at Mar-gl\_2709, Mar-gl\_2973, and Mar-gl\_3215 respectively). This dataset of overestimated  
448 temperatures led to significantly lower calibration parameters compared to the measured  
449 temperature dataset. Moreover, including critical points close to the lower margin of the glacier  
450 (Mar-gl\_2709 in summer 2010) led to wrong calibration at the other two points, which are likely to  
451 have a higher spatial representativeness given the larger distance from the glacier margin.

452 The calibration parameters obtained with the G&B temperature dataset were closer to those  
453 obtained with the measured temperature dataset, as could be expected given the smaller errors in  
454 temperature estimations (Fig. 9). In summer 2010, modeling results with the G&B temperature  
455 dataset were also the best among the three tested methods for air temperature calculation, in both  
456 calibration and validation runs. The same cannot be stated for summer 2011, due to the larger  
457 temperature underestimation at Mar-gl\_3140 and Car-gl\_3144. Similar errors occurring at Mar-  
458 gl\_3438 did not impact mass balance estimations because they mainly happened at below-zero  
459 temperatures (Fig. 9).

460 The S&M temperature dataset led to the worst results in summer 2010 due to the strong  
461 underestimation of air temperature at Mar-gl\_2709 (-1.6°C). Calibrated parameters in 2010 were  
462 thus overestimated and led to mass balances that were too negative, on average, in 2011. On the  
463 contrary, when used for calibration, the data of 2011 led to parameters much closer to the measured  
464 temperature dataset, leading to correct mass balance estimations in summer 2010 with the exception  
465 of the already mentioned Mar-gl\_2709.

466

#### 467 **5 Discussion**

468 The temperature distribution and wind regime were found to be remarkably different for the three  
469 investigated glaciers (Tables 2 and 4, Fig. 4). The most significant differences were detected  
470 between La Mare Glacier, where the KBL and the cooling effect were clearly recognizable, and the  
471 Careser Occidentale Glacier, where the air temperature was not significantly different from the  
472 ambient temperature and where prevailing up-glacier winds (i.e. valley winds) dominated.  
473 Differences were even more prominent during warm and stable weather (Fig. 5), brought by  
474 persistent anticyclonic systems (as detected by inspection of reanalysis weather charts from  
475 [www.wetterzentrale.de](http://www.wetterzentrale.de), last access: 31 October 2014).

476

477 The Car-gl\_3082 site, on Careser Orientale Glacier, also displayed peculiar conditions compared to  
478 most weather stations operated on La Mare Glacier. On the one hand a prevailing up-glacier wind  
479 was recognized, but it cannot be attributed unequivocally to valley winds because the direction  
480 roughly corresponds to prevailing synoptic winds in the Ortles-Cevedale area (Gabrieli et al., 2011).  
481 On the other hand, although katabatic flows were generally absent, this site was the coldest in  
482 summer 2011, exhibiting a mean depression of 1°C compared to the ambient temperature (Table 4).  
483 In addition, during warm anticyclonic periods it displayed a cooling effect similar to Mar-gl\_2973  
484 and Mar-gl\_3140, located in the middle part of La Mare Glacier. This is unusual for locations close  
485 to the top of glacier flowlines, which normally display a low cooling effect and high temperature  
486 sensitivity (e.g. Greuell and Böhm, 1998; Shea and Moore, 2010; Petersen et al., 2013). The  
487 efficient cooling at Car-gl\_3082 could have been caused by the combination of adiabatic cooling of  
488 ascending air and cooling by loss of sensible heat due to the rather long fetch (780 m from the lower  
489 edge of the glacier), whereas in katabatic flows the loss of sensible heat is to some extent  
490 compensated by the adiabatic heating of descending air.

491 The behavior of the two weather stations on Careser Occidentale and Orientale glaciers provides  
492 evidence of the reduced effectiveness of small glaciers (deriving from the fragmentation of larger  
493 glaciers) in cooling the air above, compared to wider glaciers or wider portions of the same parent  
494 glacier. This is suggested by the fact that these two weather stations, despite being at almost the  
495 same flow path distance from the upper glacier margin (Table 1, Fig. 2), have very different cooling  
496 effects (Table 4, Fig. 4), which largely explain errors in modeled ablation rates (Fig. 10; Figure 8  
497 from Carturan et al., 2012).

498 In consideration of the high number and contribution to the world's total ice volume of smaller  
499 glaciers (Haeberli et al., 1989; Paul et al., 2004; Zemp et al., 2008; Bahr and Radić, 2012), and  
500 given the absence of previous experimental data from such small ice bodies, these results provide a  
501 first quantification for an important reinforcing mechanism during glacier decay, that is, the  
502 disintegration of parent glaciers into smaller units, which have reduced effectiveness in cooling the  
503 air above and in triggering katabatic flows. Clearly, these results are not conclusive and require  
504 further experimental data to assess their generalizability, and to develop generalized strategies for  
505 calculating air temperature over glaciers with similar characteristics, to be implemented in  
506 distributed mass balance models.

507 A clear dependency of air temperature on elevation was found on La Mare Glacier, where the  
508 weather stations were placed along a longitudinal profile, exploring a large range of elevations (Fig.  
509 3). The on-glacier lapse rate was steeper than the standard ambient lapse rate, unlike in previous  
510 works which mostly report lower values, ranging from -2.8 to -8.1°C km<sup>-1</sup> and averaging -4.9°C  
511 km<sup>-1</sup> (Petersen and Pellicciotti, 2011, and references cited therein; Petersen et al., 2013). The high  
512 lapse rate measured on La Mare Glacier is likely due to its physical characteristics and to the  
513 specific location of weather stations. For example, Mar-gl\_2973, which is located 2.13 km  
514 downslope from the upper margin of the glacier, displayed only a moderate cooling effect (-0.74°C  
515 in 2010 and - 0.90°C in 2011), due to the presence of a steep slope causing adiabatic heating right  
516 above the weather station. An even more unusual behavior was measured at Mar-gl\_2709, close to  
517 the terminus of the glacier. Here the cooling effect was detected only during daytime, with valley  
518 winds prevailing over katabatic winds, while at night the adiabatic heating of the air descending the  
519 steep tongue prevailed over the cooling due to turbulent exchanges. Besides the physical  
520 characteristics of the glacier, however, the steep lapse rates might also have been influenced by the  
521 high lapse rate measured outside the thermal influence of glaciers.

522 The specific reasons for the steepness of the high-altitude ambient lapse rates are not easy to  
523 identify. According to Marshall et al. (2007) and Minder et al. (2010), for example, they could have  
524 been caused by the prevailing synoptic circulation, local energy balance regime, persistence of

525 snow cover, geographic position (windward or leeward with respect to the prevailing synoptic  
526 wind). Apart from these considerations, it has to be noted that the interpolation and extrapolation of  
527 ambient temperature at high altitudes, as a starting point for the computation of the on-glacier  
528 temperature fields, are strongly dependent on the availability and/or selection of suitable weather  
529 stations. As already suggested e.g. by Oerlemans, (2001), measurements from high-altitude weather  
530 stations are preferable to measurements from valley-floor sites, which are prone to thermal  
531 inversions and subject to high temperature oscillations during the day.

532 The good alignment of our data points with the transfer functions of Shea and Moore (2010), which  
533 can be seen in Fig. 6, is remarkable given the different characteristics of glaciers and geographic  
534 setting of the two study areas. This result points to a good generalizability of the S&M method,  
535 which we have tried to improve by implementing a transfer function for  $T^*$  based on the *FPL* rather  
536 than on elevation. The S&M method was fairly successful at sites where the KBL was detected  
537 (Mar-gl\_3140, Mar-gl\_3215), that is, for the conditions under which the method has been  
538 implemented. Nevertheless, at Mar-gl\_2973 it significantly underestimated the temperature,  
539 probably because it does not account for gradients upslope of the weather station, which causes a  
540 local prevalence of adiabatic heating. A larger error occurred at Mar-gl\_2709, which is however  
541 influenced by valley winds and thermal emission from the surrounding bare rocks, determining high  
542 temperature sensitivity and unusual  $T^*$  at such a long FPL (2896 m, Fig. 6). With this method it was  
543 not possible to reproduce the temperature differences between Car-gl\_3082 and Car-gl\_3144, as  
544 expected, because they have similar values of down-glacier FPL (313 and 354 m, respectively).

545 The G&B method provided the best overall results. Among sites with prevailing katabatic winds,  
546 the improvement was clearest at Mar-gl\_2973, where the method was able to account for the  
547 combined effect of adiabatic heating and turbulent exchanges, which were regulated by the slope  
548 variations along the upstream flowline. On the other hand, it was worse than the S&M method at  
549 distinguishing between the two Careser glaciers, and the better results in terms of lower mean errors  
550 at Mar-gl\_2709, Mar-gl\_3438 and Car-gl\_3082, compared to the S&M method, are coincidental  
551 because at these sites the KBL was almost absent or not prevailing.

552 Other combinations of parameters  $x_0$  and  $L_R$  have been tested to evaluate whether they are valid  
553 alternatives, for example for eliminating the artificial step in calculated versus observed temperature  
554 at Mar-gl\_2973 and Mar-gl\_2709 (Fig. 9), caused by the jump of  $x_0$  from 0 to 1440 m when the  
555 freezing level exceeds the top of the flowline. The tested combinations were: i)  $x_0 = 0$  m (constant)  
556 and  $L_R = 8340$  m, ii)  $x_0 = 1440$  m (constant) and  $L_R = 8340$  m, and iii)  $x_0 = 1835$  m (constant) and  $L_R$   
557  $= 12682$  m. The last combination results from the best fit to AVDM data in Fig. 8, excluding the  
558 outlier Mar-gl\_2709. We also tested the calculation using the unmodified ambient temperature.  
559 Tests indicate that at sites with almost no cooling effect (Mar-gl\_3438 and Car-gl\_3144) the  
560 unmodified ambient temperature or the combination i) ( $x_0 = 0$ ) provide the best results (mean errors  
561  $< 0.2^\circ\text{C}$  in absolute value). At the four sites with prevailing KBL the best overall solution was iii),  
562 but this combination is specific for the AVDM and not generalizable, due to the rather small size of  
563 our glaciers. At Mar-gl\_2973, options ii) and iii) completely removed the step and provided the best  
564 statistics. At Mar-gl\_3215, option iii) provided almost identical results to a variable  $x_0$ , while  
565 options i) and ii) led to excessive overestimations and underestimations, respectively. At Mar-  
566 gl\_3140, the best option was iii).

567 These findings highlight site-specific and glacier-specific conditions which still need investigation  
568 in order to generalize the G&B procedure, possibly by including smaller or disintegrating glaciers  
569 in the datasets used for the generalization. Sites where the KBL no longer exists and is replaced by  
570 prevailing valley winds and/or synoptic winds also need to be included as they reveal important  
571 controlling mechanisms during glacier shrinking, which require modifications to the main G&B  
572 algorithms in order to be taken into account.

573 The results of EISModel applications underline the importance of correct on-glacier air temperature  
574 estimation for reliable mass balance calculations (Table 5, Fig. 10). Even small estimation errors  
575 induce significant distortions in calibration parameters and compromise model generalizability. The  
576 2010 dataset on La Mare Glacier clearly demonstrates how single points, especially if they are  
577 displaced along altitudinal profiles, can affect the calibration of the model and its capability to  
578 account for the vertical gradients of the mass balance. This problem is clearly emphasized in our  
579 case study, with only three weather stations along the flowline of La Mare Glacier in 2010. The  
580 spatial representativeness of Mar-gl\_2973 and Mar-gl\_3215 is likely much higher than that of Mar-  
581 gl\_2709, at the glacier terminus, which reflects the conditions close to the lower edge of glaciers.  
582 However, mass balance models should be improved in order to account for the decreased thermal  
583 offset in these areas and in smaller glacier units resulting from the fragmentation of larger glaciers,  
584 because they represent important processes involved in the response of glaciers to climatic changes.

585

## 586 **6 Concluding remarks**

587 The results of this work have interesting implications for the knowledge of glacier's reactions to  
588 climatic changes, and for their modeling. The main conclusions from this study are the following:

- 589 1) our findings provide a first experimental evidence for the reduced effectiveness of small  
590 glaciers ( $< 0.5 \text{ km}^2$ ) in cooling the air above and in triggering katabatic flows. This  
591 represents an important reinforcing mechanism during glacier decay and fragmentation.
- 592 2) a good match between our temperature measurements and the parameterizations proposed  
593 by Shea and Moore (2010) and, best of all, Greuell and Böhm (1998) was found, at least for  
594 the on-glacier weather stations where katabatic flows prevail. This represents a step forward  
595 for the generalization of these methods, which on the other hand still need refinements, in  
596 particular for areas close to the margins (e.g. the front) and for the smaller units resulting  
597 from glacier fragmentation
- 598 3) even small deviations of calculated on-glacier temperature from observations significantly  
599 impacted the calibration of EISModel and its efficiency, thus confirming that accurate  
600 temperature estimations are an essential prerequisite for model development, calibration and  
601 generalizability.

602

## 603 **Author contribution**

604 L. Carturan, F. Cazorzi and G. Dalla Fontana designed the glacio-meteorological experiment and  
605 carried it out. L. Carturan and F. De Blasi processed and analyzed the experimental data. F. Cazorzi  
606 and L. Carturan developed the EISModel and performed the glacier mass balance simulations. L.  
607 Carturan prepared the manuscript with contributions from all co-authors.

## 608 **Acknowledgments**

609 The data and the mass balance model used in this study can be made available upon request to the  
610 authors. This study was funded by the Italian MIUR Project (PRIN 2010-11): "Response of  
611 morphoclimatic system dynamics to global changes and related geomorphological hazards" (local  
612 and national coordinators G. Dalla Fontana and C. Baroni). The authors acknowledge the  
613 Autonomous Province of Trento and Enel SpA for providing the meteorological and topographic  
614 data. Special thanks to Vinicio Carraro for the help in the setup of automatic weather stations, and  
615 to the students, colleagues and alpine guides who have contributed to the field surveys. Finally,

616 thanks to the scientific editor V. Radić and to two anonymous reviewers, whose comments were  
617 helpful for finalizing the paper.

618

## 619 **References**

620 Abbate, S., Avvenuti, M., Carturan, L., and Cesarini, D.: Deploying a communicating automatic  
621 weather station on an Alpine Glacier, *Procedia Comput. Sci.*, 19, 1190–1195, 2013.

622 Bahr, D. B., and Radić, V.: Significant contribution to total mass from very small glaciers. *The*  
623 *Cryosphere*, 6, 763–770, 2012.

624 Barry, R. G.: The status of research on glaciers and global glacier recession: a review, *Prog. Phys.*  
625 *Geog.*, 30(3), 285-306, 2006.

626 Braithwaite, R. J.: Regional modelling of ablation in West Greenland, *Grøn. Geol. Unders. Rapp.*  
627 98, 20 pp., 1980.

628 Braithwaite, R. J., Zhang, Y., and Raper, S. C. B.: Temperature sensitivity of the mass balance of  
629 mountain glaciers and icecaps as a climatological characteristic, *Z. Gletscherkunde Glazialgeol.*, 38,  
630 35–61, 2002.

631 Carturan, L.: Climate change effects on the cryosphere and hydrology of a high-altitude watershed.  
632 PhD diss., TeSAF - University of Padova, Italy, 2010.

633 Carturan, L., Dalla Fontana, G., and Cazorzi, F.: The mass balance of La Mare Glacier (Ortles-  
634 Cevedale, Italian Alps) from 2003 to 2008, in: *Epitome - Geoitalia 2009*, Settimo Forum Italiano di  
635 Scienze della Terra, Rimini, Italy, 9–11 September 2009, Vol. 3, p. 298, 2009.

636 Carturan, L., Cazorzi, F., and Dalla Fontana, G.: Distributed mass-balance modeling on two  
637 neighboring glaciers in Ortles-Cevedale, Italy, from 2004 to 2009, *J. Glaciol.*, 58(209), 467-486,  
638 2012a.

639 Carturan L., Dalla Fontana, G., and Borga, M.: Estimation of winter precipitation in a high-altitude  
640 catchment of the Eastern Italian Alps: validation by means of glacier mass balance observations,  
641 *Geogr. Fis. Din. Quat.*, 35, 37-48, 2012b.

642 Carturan, L., Baroni, C., Becker, M., Bellin, A., Cainelli, O., Carton, A., Casarotto, C., Dalla  
643 Fontana, G., Godio, A., Martinelli, T., Salvatore, M. C., and Seppi R.: Decay of a long-term  
644 monitored glacier: Careser Glacier (Ortles-Cevedale, European Alps), *The Cryosphere*, 7, 1819-  
645 1838, 2013.

646 Carturan L., Baroni, C., Carton, A., Cazorzi, F., Dalla Fontana, G., Delpero, C., Salvatore, M. C.,  
647 Seppi, R., and Zanoner, T.: Reconstructing fluctuations of La Mare Glacier (Eastern Italian Alps) in  
648 the Late Holocene: new evidences for a Little Ice Age maximum around 1600 AD, *Geografiska*  
649 *Annaler: Series A, Physical Geography*, 96, 287-306, 2014.

650 Cazorzi, F. and Dalla Fontana, G.: Snowmelt modeling by combining air temperature and a  
651 distributed radiation index, *J. Hydrol.*, 181(1–4), 169–187, 1996.

652 Charbonneau, R., Lardeau, J. P., and Obled, C.: Problems of modelling a high mountainous  
653 drainage basin with predominant snow yields, *Hydrol. Sci. Bull.*, 26(4), 345–361, 1981.

- 654 Davidovich, N. V. and Ananicheva, M. D.: Prediction of possible changes in glacio-hydrological  
655 characteristics under global warming: Southeastern Alaska, USA, *J. Glaciol.*, 42(142), 407-412,  
656 1996.
- 657 Eriksson, B. E.: Glaciological investigations in Jotunheimen and Sarek in the years 1955 to 1957.  
658 *Geographica*, 34, 208 pp., 1958.
- 659 Fischer, A.: Glaciers and climate change: Interpretation of 50 years of direct mass balance of  
660 Hintereisferner, *Global Planet. Change*, 71 (1-2), 13-26, 2010.
- 661 Gabrieli J., Carturan, L., Gabrielli, P., Turetta, C., Cozzi, G., Staffler, H., Dinale, R., Dalla Fontana,  
662 G., Thompson, L., and Barbante, C.: Impact of Po Valley emissions on the highest glacier of the  
663 Eastern European Alps, *Atmos. Chem. Phys.*, 11, 8087–8102, 2011.
- 664 Gardner, A. S. and Sharp, M. J.: Sensitivity of net mass-balance estimates to near-surface  
665 temperature lapse rates when employing the degree-day method to estimate glacier melt, *Ann.*  
666 *Glaciol.*, 50, 80–86, 2009.
- 667 Gardner, A. S., Sharp, M. J., Koerner, R. M., Labine, C., Boon, S., Marshall, S. J., Burgess, D. O.,  
668 and Lewis, D.: Near-surface temperature lapse rates over arctic glaciers and their implications for  
669 temperature downscaling, *J. Clim.*, 22, 4281–4298, 2009.
- 670 Georges, C. and Kaser, G.: Ventilated and unventilated air temperature measurements for glacier-  
671 climate studies on a tropical high mountain site, *J. Geophys. Res.*, 107(D24), 4775,  
672 doi:10.1029/2002JD002503, 2002.
- 673 Greuell, W. and Böhm, R.: 2m temperatures along melting midlatitude glaciers, and implications  
674 for the sensitivity of the mass balance to variations in temperature, *J. Glaciol.*, 44(146), 9–20, 1998.
- 675 Greuell, W., Knap, W. H., and Smeets, P. C.: Elevational changes in meteorological variables along  
676 a mid-latitude glacier during summer, *J. Geophys. Res.*, 102(D22), 25941–25954, doi:  
677 10.1029/97JD02083, 1997.
- 678 Haeberli, W., Bosch, H., Scherler, K., Østrem, G. and Wallén, C. (eds): *World Glacier Inventory:*  
679 *Status 1988.* IAHS(ICSU)/UNEP/UNESCO/World Glacier Monitoring Service, Nairobi, 1989.
- 680 Haeberli, W., Hoelzle, M., Paul, F., and Zemp, M.: Integrated monitoring of mountain glaciers as  
681 key indicators of global climate change: the European Alps, *Ann. Glaciol.*, 46(1), 150-160, 2007.
- 682 Havens, J. M.: Climatological Notes from Axel Heiberg Island, NWT, Canada, *Arctic*, 17(4), 261-  
683 263, 1964.
- 684 Hock, R.: Glacier melt: a review of processes and their modelling, *Prog. Phys. Geog.*, 29(3), 362-  
685 391, 2005.
- 686 Huss, M., Bauder, A., and Funk, M.: Homogenization of longterm mass-balance time series, *Ann.*  
687 *Glaciol.*, 50(50), 198–206, 2009.
- 688 Khodakov, V. G.: Glaciers as water resource indicators of the glacial areas of the USSR.  
689 *International Association of Hydrological Sciences Publication*, 104, 22-29, 1975.
- 690 Klok, E. J. and Oerlemans, J.: Modelled climate sensitivity of the mass balance of  
691 Morteratschgletscher and its dependence on albedo parameterization, *Int. J. Climatol.*, 24, 231–245,  
692 2004.



- 693 Machguth, H., Purves, R. S., Oerlemans, J., Hoelzle, M., and Paul, F.: Exploring uncertainty in  
694 glacier mass balance modelling with Monte Carlo simulation, *The Cryosphere*, 2, 191-204, 2008.
- 695 Marshall, S. J., Sharp, M. J., Burgess, D. O., and Anslow, F. S.: Near surface-temperature lapse  
696 rates on the Prince of Wales Icefield, Ellesmere Island, Canada: implications for regional  
697 downscaling of temperature, *Int. J. Climatol.*, 27(3), 385–398, 2007.
- 698 Michlmayr, G., Lehning, M., Kobltschnig, G., Holzmann, H., Zappa, M., Mott, R., and Schoner,  
699 W.: Application of the alpine 3D model for glacier mass balance and glacier runoff studies at  
700 Goldbergkees, Austria, *Hydrol. Process.*, 22, 3941–3949, 2008.
- 701 Minder, J. R., Mote, P. W., and Lundquist, J. D.: Surface temperature lapse rates over complex  
702 terrain: Lessons from the Cascade Mountains, *J. Geophys. Res.*, 115, D14122, doi:  
703 10.1029/2009JD013493, 2010.
- 704 Nash, J. E. and Sutcliffe, J. V.: River flow forecasting through conceptual models. Part 1. A  
705 discussion of principles, *J. Hydrol.*, 10(3), 282–290, 1970.
- 706 Nolin, A., Philippe, J., Jefferson, A., and Lewis, S. L.: Present-day and future contributions of  
707 glacier runoff to summertime flows in a Pacific Northwest watershed: Implications for water  
708 resources, *Water Resour. Res.*, 46, W12509, doi: 10.1029/2009WR008968, 2010.
- 709 Oerlemans, J.: *Glaciers and climate change*, AA Balkema, Lisse, 2001.
- 710 Paul, F.: The influence of changes in glacier extent and surface elevation on modeled mass balance,  
711 *The Cryosphere*, 4, 569-581, 2010.
- 712 Paul, F., Kääb, A., Maisch, M., Kellenberger, T. and Haeberli, W.: Rapid disintegration of Alpine  
713 glaciers observed with satellite data. *Geophys. Res. Lett.*, 31, L21402, 2004.
- 714 Paul, F., Machguth, H., and Kääb, A.: On the impact of glacier albedo under conditions of extreme  
715 glacier melt: the summer of 2003 in the Alps, *EARSeL eProc.*, 4(2), 139–149, 2005.
- 716 Petersen, L. and Pellicciotti, F.: Spatial and temporal variability of air temperature on a melting  
717 glacier: atmospheric controls, extrapolation methods and their effect on melt modeling, *Juncal  
718 Norte Glacier, Chile*, *J. Geophys. Res.*, 116(D23), D23109, doi: 10.1029/2011JD015842, 2011.
- 719 Petersen, L., Pellicciotti, F., Juszak, I., Carenzo, M., and Brock, B.: Suitability of a constant air  
720 temperature lapse rate over an Alpine glacier: testing the Greuell and Böhm model as an alternative,  
721 *Ann. Glaciol.*, 54(63), 120-130, 2013.
- 722 Raymond, C. F. and Neumann, T. A.: Retreat of Glaciar Tyndall, Patagonia, over the last half-  
723 century, *J. Glaciol.*, 51(173), 239–247, 2005.
- 724 Savenije, H. H. G.: Equifinality, a blessing in disguise? *Hydrol. Process.*, 15(14), 2835–2838, 2001.
- 725 Schytt, V.: *Glaciological investigations in the Thule camp area*, S.I.P.R.E. Report No. 28, 88 pp.,  
726 1955.
- 727 Shea, J. M. and Moore, R. D.: Prediction of spatially distributed regional-scale fields of air  
728 temperature and vapor pressure over mountain glaciers, *J. Geophys. Res.*, 115, D23107,  
729 doi:10.1029/2010JD014351, 2010.
- 730 Sivapalan, M.: Pattern, process and function: elements of a unified theory of hydrology at the  
731 catchment scale, in: *Encyclopedia of hydrological sciences*, Anderson, M. G. and McDonnell, J. J.  
732 eds., Vol. 1. Wiley, Chichester, 193–219, 2006.

- 733 Small, E. E.: Hypsometric forcing of stagnant ice margins: Pleistocene valley glaciers, San Juan  
734 Mountains, Colorado, *Geomorphology*, 14, 109–121, 1995.
- 735 Strasser, U., Corripio, J., Pellicciotti, F., Burlando, P., Brock, B., and Funk, M.: Spatial and  
736 temporal variability of meteorological variables at Haut Glacier d’Arolla (Switzerland) during the  
737 ablation season 2001: measurements and simulations, *J. Geophys. Res.*, 109(D3), D3103, doi:  
738 10.1029/2003JD003973, 2004.
- 739 Tarboton, D. G., Bras, R. L., and Rodriguez-Iturbe, I.: On the extraction of channel networks from  
740 digital elevation data. *Hydrol. Process.*, 5(1), 81-100, 1991.
- 741 Thibert, E., Blanc, R., Vincent, C., and Eckert, N.: Glaciological and volumetric mass-balance  
742 measurements: error analysis over 51 years for Glacier de Sarennes, French Alps, *J. Glaciol.*,  
743 54(186), 522–532, 2008.
- 744 van den Broeke, M. R.: Momentum, heat, and moisture budgets of the katabatic wind layer over a  
745 midlatitude glacier in summer, *J. Appl. Meteorol.*, 36(6), 763-774, 1997.
- 746 World Meteorology Organization (WMO): Intercomparison of models for snowmelt runoff,  
747 Operational Hydrology Report 23 (WMO no. 646), 1986.
- 748 Zanon, G.: Recent glaciological research in the Ortles- Cevedale region (Italian Alps), *Geogr. Fis.*  
749 *Din. Quat.*, 5(1), 75–81, 1982.
- 750 Zemp, M., Paul, F., Hoelzle, M. and Haeberli, W.: Glacier fluctuations in the European Alps 1850–  
751 2000: an overview and spatio-temporal analysis of available data. In: Orlove, B., Wiegandt, E. and  
752 Luckman B., (eds), *The Darkening Peaks: Glacial Retreat in Scientific and Social Context*.  
753 University of California Press, Berkeley, 152–167, 2008.
- 754

## Tables

756 **Table 1.** Location, flow path length (*FPL*), period of observation and used variables for glacier and  
 757 ambient weather stations<sup>a</sup>. The periods with common records are 3 July to 23 September 2010 and 7  
 758 July to 12 September 2011.

Weather station	Easting (m)	Northing (m)	Elevation (m a.s.l.)	<i>FPL</i> (m)	Period of observation		Used variables
					Summer 2010	Summer 2011	
La Mare Glacier							
<b>Mar-gl_2709</b>	626692	5143668	2709	2896	x		T, W
<b>Mar-gl_2973</b>	625960	5143483	2973	2132	x	x	T, W
<b>Mar-gl_3215</b>	625205	5143101	3215	1278	x		T, W
<b>Mar-gl_3140</b>	625290	5143523	3140	805		x	T, W
<b>Mar-gl_3438</b>	624199	5142924	3438	40	damaged	x	T, W
Careser Glacier							
<b>Car-gl_3082</b>	632283	5145512	3082	313		x	T, W
<b>Car-gl_3144</b>	629690	5145375	3144	354		x	T, W
Ambient weather stations							
Cog_1202	629915	5135988	1202	\	x	x	T
Car_2607	630570	5142410	2607	\	x	x	T, P
Car_3051	630799	5145553	3051	\	x	x	T
Bel_3328	624957	5151212	3328	\	x	x	T

759 <sup>a</sup>T = air temperature, W = wind speed and direction, P = precipitation. On-glacier sites are in bold  
 760 type.

761

762

763

764

765

766

767

768

769

770

771

772

773

774

775

776 **Table 2.** Descriptive statistics for air temperature data recorded by the weather stations. On-glacier  
 777 sites are in bold type.

Weather station	Minimum	Maximum	Mean	Standard deviation	Mean daily range
Summer 2010					
<b>Mar-gl_2709</b>	-1.9	14.2	5.9	3.3	2.2
<b>Mar-gl_2973</b>	-4.4	11.6	3.8	3.1	2.5
<b>Mar-gl_3215</b>	-6.6	10.6	2.2	3.4	2.9
Cog_1202	2.3	29.8	14.8	5.5	10.2
Car_2607	-2.4	18.4	7.3	4.1	4.6
Car_3051	-5.6	14.1	3.9	4.0	2.8
Bel_3328	-10.5	13.9	1.5	4.5	3.6
Summer 2011					
<b>Mar-gl_2973</b>	-4.8	12.0	4.3	2.7	2.6
<b>Mar-gl_3140</b>	-6.2	9.7	3.3	2.8	2.1
<b>Mar-gl_3438</b>	-7.9	9.5	1.1	3.1	3.2
<b>Car-gl_3082</b>	-6.0	10.8	3.3	2.9	2.6
<b>Car-gl_3144</b>	-6.1	10.9	3.5	3.1	2.3
Cog_1202	4.0	29.8	15.4	4.9	10.5
Car_2607	-0.9	19.5	8.1	3.6	4.9
Car_3051	-5.3	13.7	4.6	3.5	2.8
Bel_3328	-8.2	13.5	2.1	3.8	3.5

778

779

780

781

782

783

784

785

786

787

788

789

790

791

792

793

794

795 **Table 3.** Validation statistics for ambient temperature calculations (global dataset including summer  
796 2010 and 2011)<sup>a</sup>

Lapse rate (°C m <sup>-1</sup> )	Used weather stations	Calculation of air temperature at Car_3051			Calculation of air temperature at Bel_3328		
		Mean Error (°C)	RMSE (°C)	N&S index	Mean Error (°C)	RMSE (°C)	N&S index
Moist adiabatic lapse rate							
-0.0065	1	-1.14	3.81	-0.019	-0.51	3.59	0.276
-0.0065	2	0.59	1.32	<b>0.878</b>	1.22	2.02	0.771
-0.0065	3	\	\	\	0.63	1.46	<b>0.880</b>
-0.0065	4	-0.63	1.46	0.851	\	\	\
Fixed calibrated lapse rate							
-0.0053	1, 2	1.13	1.64	0.812	2.11	2.65	0.605
-0.0059	1, 3	\	\	\	0.81	1.54	0.866
-0.0063	1, 4	-0.70	1.49	0.845	\	\	\
-0.0078	2, 3	\	\	\	0.27	1.34	<b>0.899</b>
-0.0082	2, 4	-0.17	1.32	<b>0.877</b>	\	\	\
-0.0057	1, 2, 3	\	\	\	0.85	1.56	0.863
-0.0061	1, 2, 4	-0.74	1.51	0.841	\	\	\
Hourly variable lapse rate							
Hourly variable	1, 2	1.13	1.55	0.831	2.11	2.89	0.529
Hourly variable	1, 3	\	\	\	0.81	1.74	0.830
Hourly variable	1, 4	-0.70	1.51	0.840	\	\	\
Hourly variable	2, 3	\	\	\	0.27	1.64	<b>0.849</b>
Hourly variable	2, 4	-0.17	1.01	<b>0.929</b>	\	\	\
Hourly variable	1, 2, 3	\	\	\	0.85	1.76	0.826
Hourly variable	1, 2, 4	-0.74	1.55	0.831	\	\	\

797 <sup>a</sup>Weather stations: 1 = Cog\_1202, 2 = Car\_2607, 3 = Car\_3051, 4 = Bel\_3328. N&S index is the  
798 efficiency criterion according to Nash and Sutcliffe (1970). Bold type indicates the best results for  
799 each tested method.

800  
801  
802  
803  
804  
805  
806  
807  
808  
809  
810  
811

812 **Table 4.** Mean values of cooling effect, wind speed and wind direction recorded at the on-glacier  
 813 weather stations.

Weather station	Mean cooling effect (°C)	Mean wind speed (m/s)	Mean wind direction (°)
Summer 2010			
Mar-gl_2709	-0.65	2.00	247
Mar-gl_2973	-0.74	3.13	230
Mar-gl_3215	-0.27	3.47	258
Summer 2011			
Mar-gl_2973	-0.90	2.82	224
Mar-gl_3140	-0.47	3.00	239
Mar-gl_3438	0.06	\	\
Car-gl_3082	-1.01	2.40	249
Car-gl_3144	-0.18	1.98	90

814  
 815  
 816  
 817  
 818  
 819  
 820  
 821  
 822  
 823  
 824  
 825  
 826  
 827  
 828  
 829  
 830  
 831  
 832  
 833  
 834

835 **Table 5.** Calibration parameters and mass balance statistics from EISModel applications with four  
 836 different datasets of air temperature<sup>a</sup>

Temperature dataset	Calibrated parameters		Calibration run (summer 2010)			Validation run (summer 2011)		
	TMF (mm h <sup>-1</sup> °C <sup>-1</sup> )	RMF (mm h <sup>-1</sup> W <sup>-1</sup> m <sup>2</sup> )	ME (m w.e.)	RMSE (m w.e.)	N&S	ME (m w.e.)	RMSE (m w.e.)	N&S
Measured temperature	0.246	0.00117	-0.027	0.080	0.992	+0.052	0.156	0.888
Standard lapse rate	0.202	0.00100	-0.049	0.252	0.918	-0.160	0.261	0.686
G&B method	0.251	0.00109	-0.006	0.113	0.984	+0.156	0.314	0.545
S&M method	0.291	0.00128	-0.049	0.359	0.832	-0.282	0.366	0.381

	Calibrated parameters		Calibration run (summer 2011)			Validation run (summer 2010)		
	TMF (mm h <sup>-1</sup> °C <sup>-1</sup> )	RMF (mm h <sup>-1</sup> W <sup>-1</sup> m <sup>2</sup> )	ME (m w.e.)	RMSE (m w.e.)	N&S	ME (m w.e.)	RMSE (m w.e.)	N&S
Measured temperature	0.246	0.00138	+0.006	0.152	0.893	-0.095	0.119	0.982
Standard lapse rate	0.175	0.00111	-0.008	0.210	0.796	+0.178	0.346	0.844
G&B method	0.265	0.00141	+0.045	0.288	0.618	-0.172	0.226	0.934
S&M method	0.236	0.00129	-0.018	0.241	0.732	+0.315	0.522	0.647

837 <sup>a</sup>Calibration in 2010 and validation in 2011 in the upper table, vice versa in the lower table.  
 838 Measured vs. modeled values are displayed in Fig. 10.

839

840

841

842

843

844

845

846

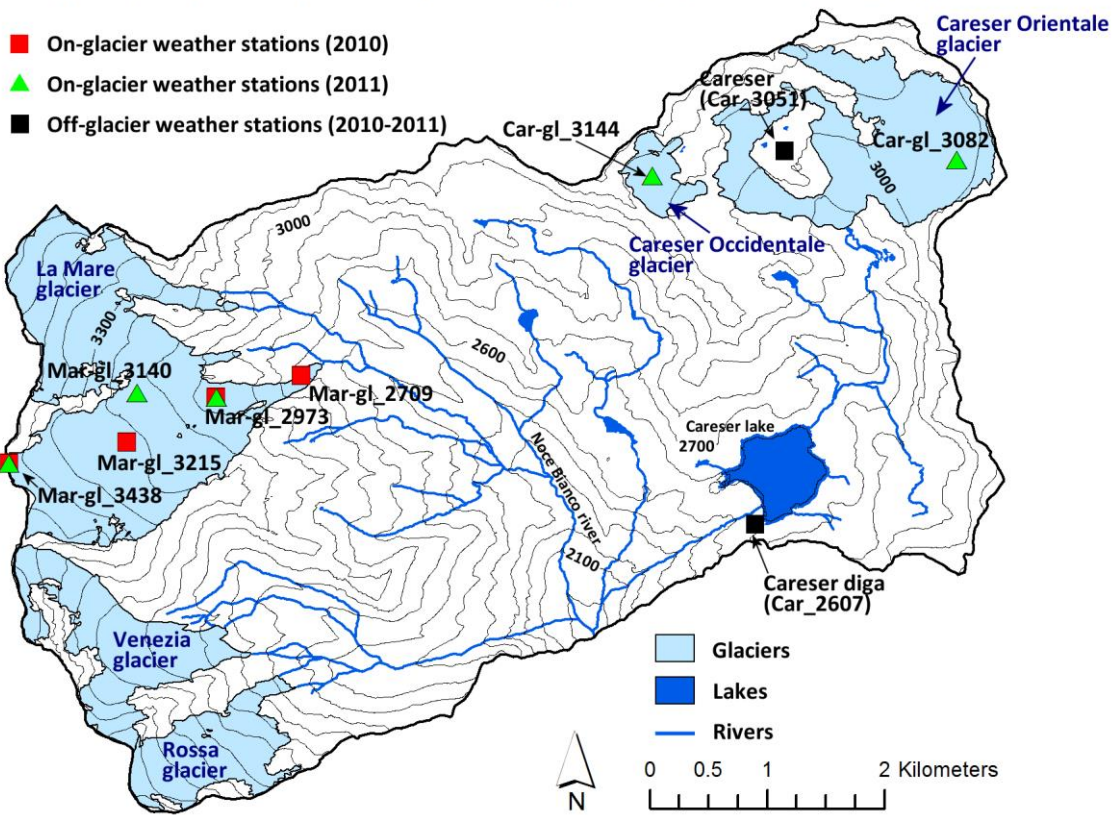
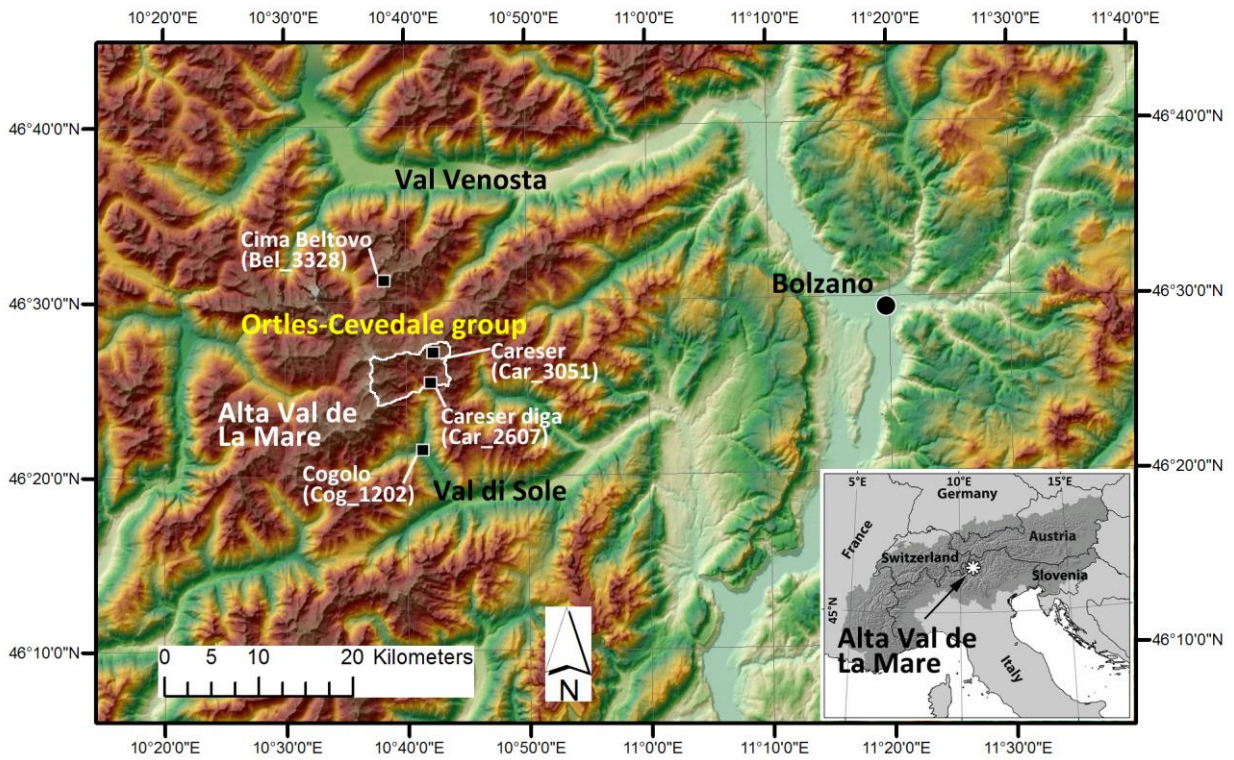
847

848

849

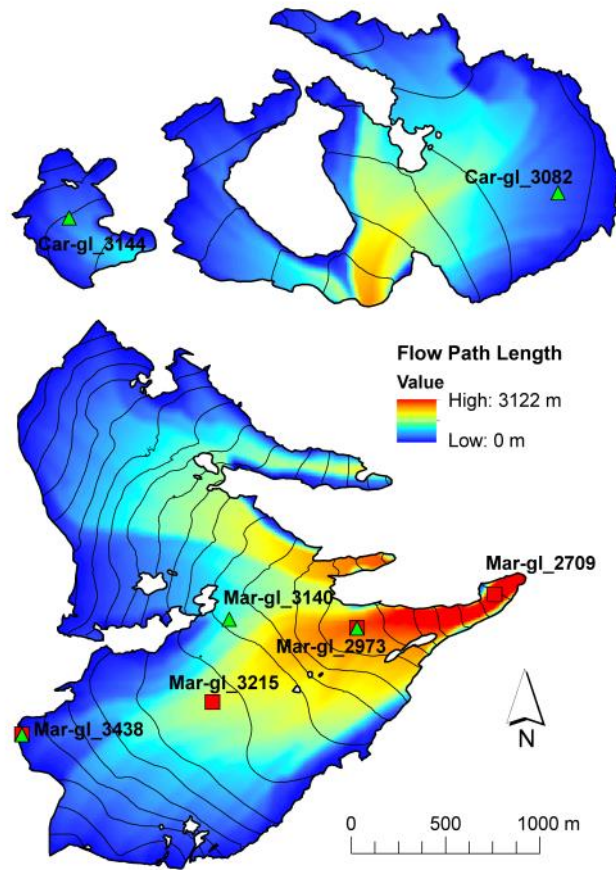
850

851



855 Figure 1 - Geographic setting of Alta Val de La Mare and location of the automatic weather stations.





858

859

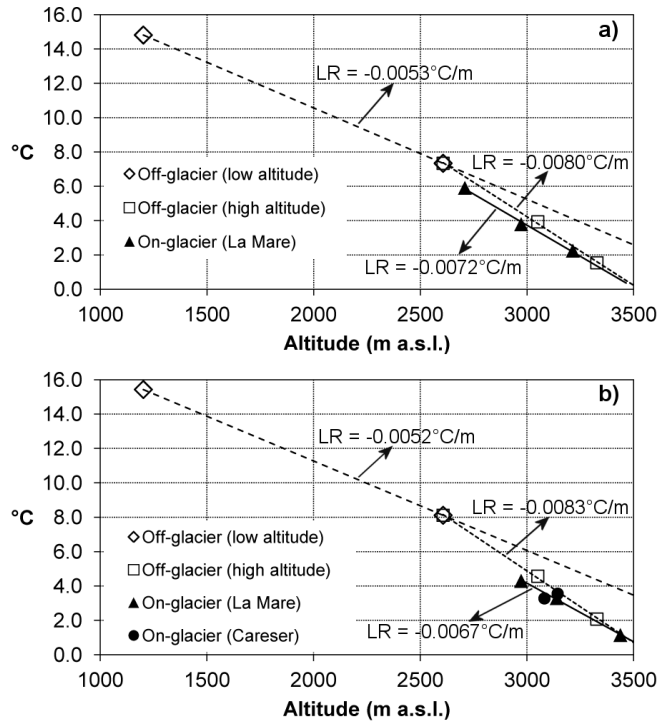
Figure 2 – Map of the flow path length calculated for Careser and La Mare glaciers.

860

861

862

863



864

865 Figure 3 - Mean temperature vs. altitude: a) from 3 July to 23 September, 2010, and b) from 7 July  
 866 to 12 September, 2011. Lines indicate linear regressions of temperature vs. altitude for subsets of  
 867 weather stations. LR = vertical lapse rates.

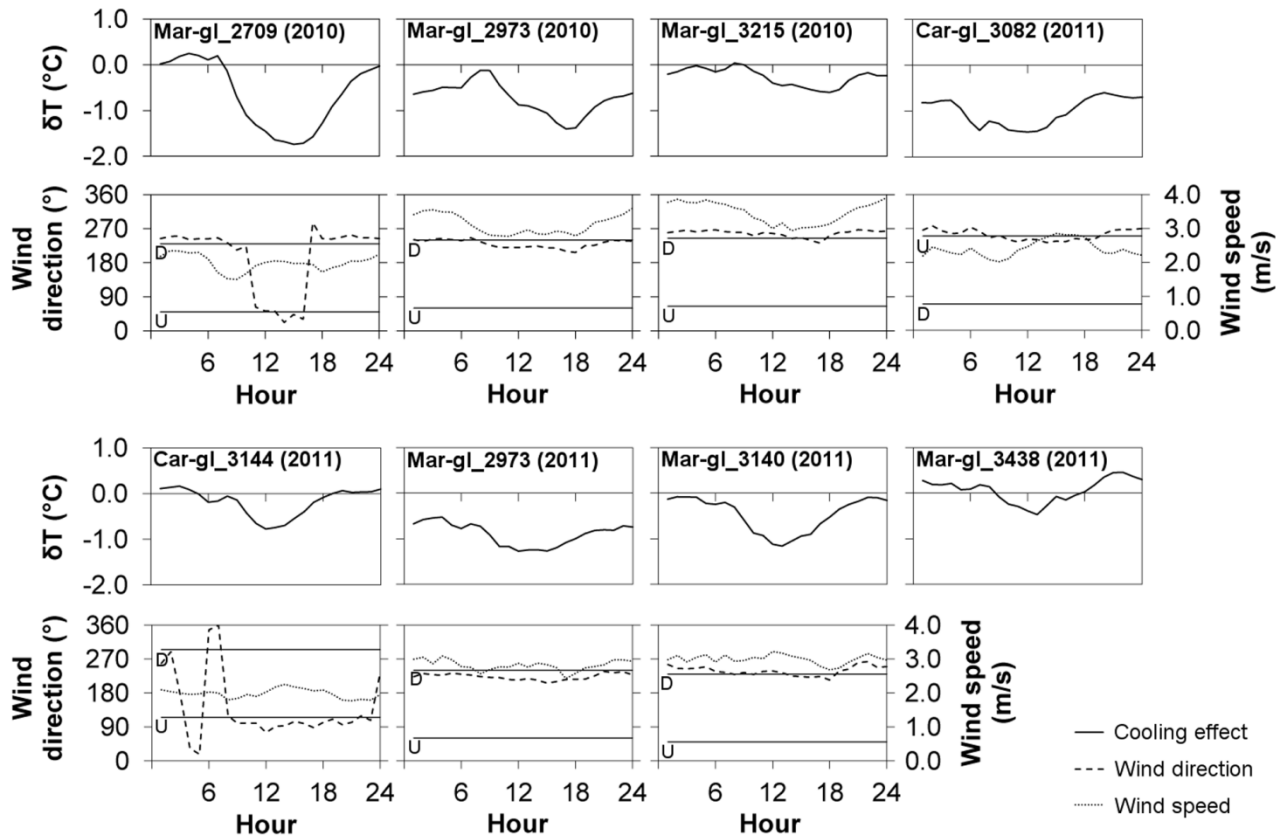
868

869

870

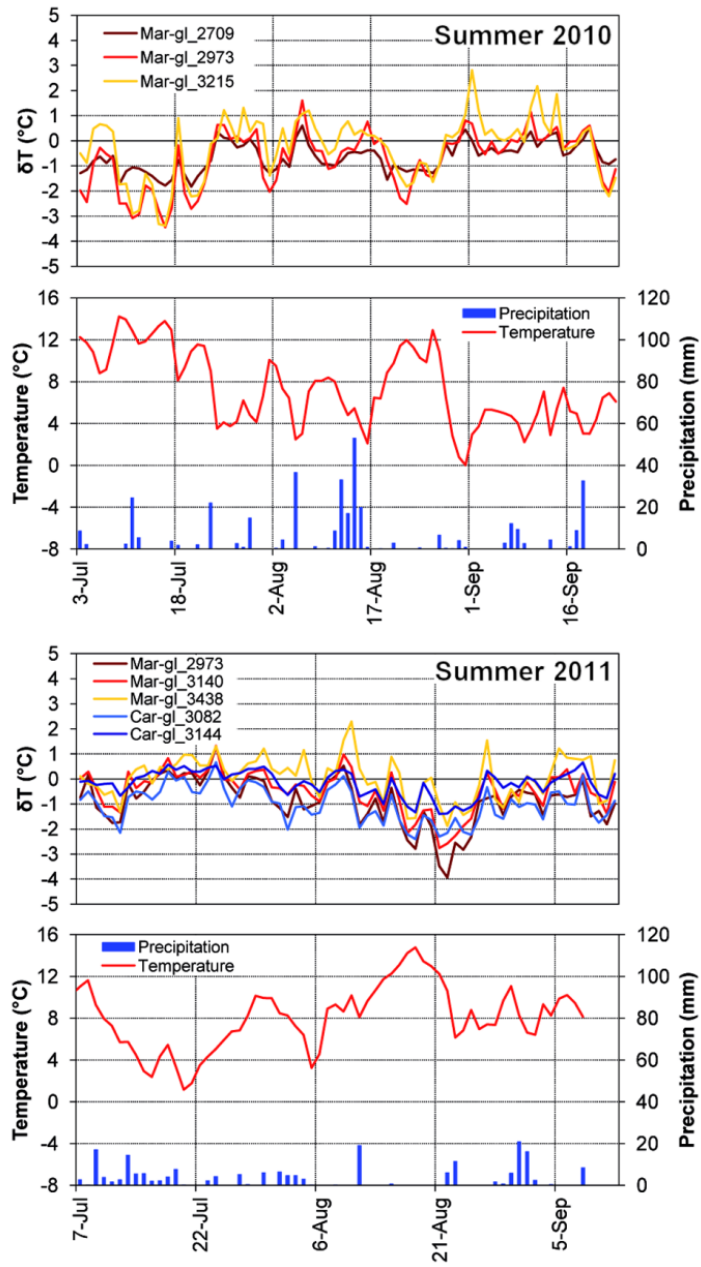
871

872



873

874 Figure 4 - Mean daily cycle of the glacier cooling effect ( $\delta T$ ), wind direction and wind speed at the  
 875 eight on-glacier weather stations. The operation period of each station is indicated in brackets.  
 876 Down-glacier and up-glacier wind directions are indicated with straight lines marked with 'D' and  
 877 'U'. Mar-gl\_3438 lacks wind data because of anemometer failure.



878

879

880

Figure 5 - Mean daily cooling effect at the on-glacier weather stations, and corresponding daily precipitation and mean temperature at Careser diga (Car\_2607).

881

882

883

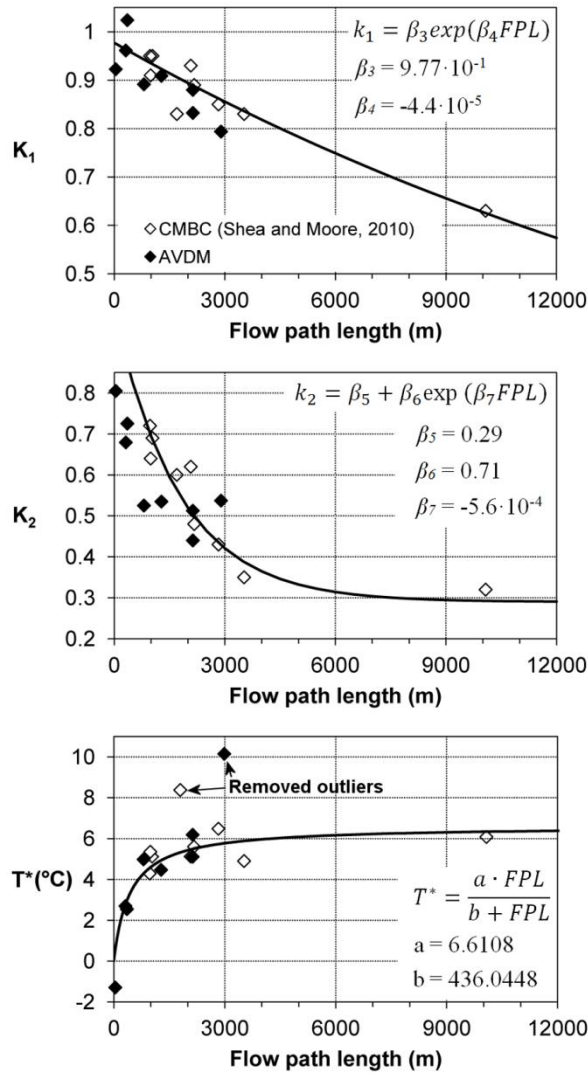
884

885

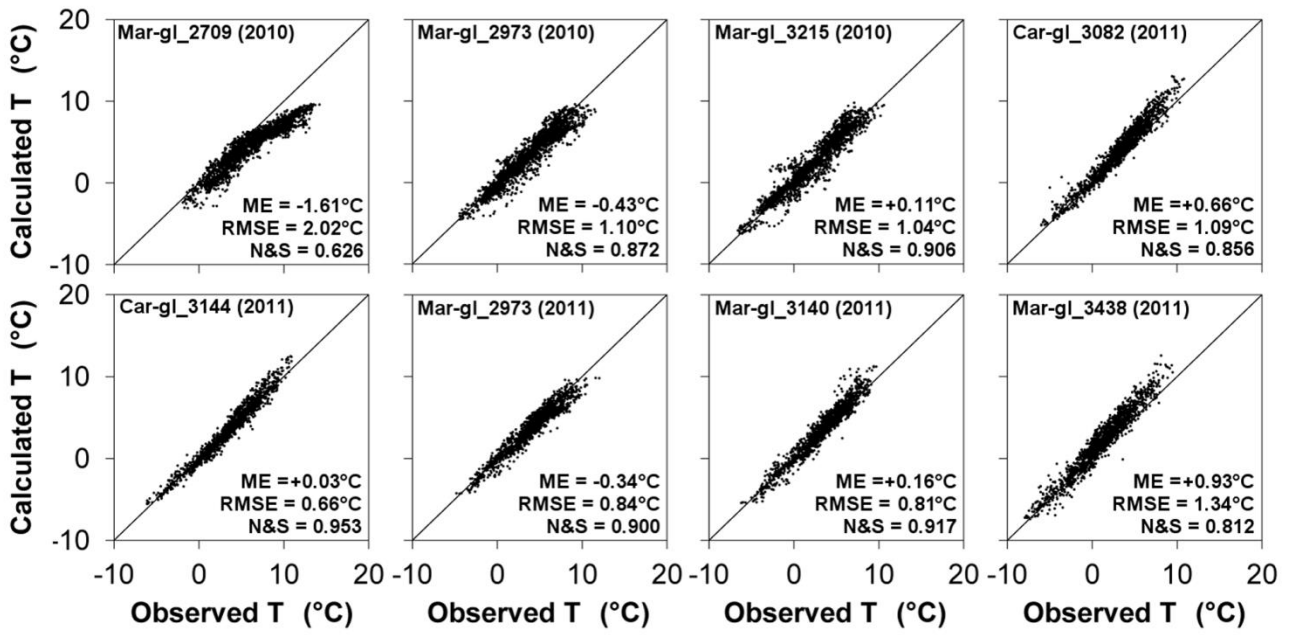
886

887

888



891 Figure 6 - Transfer functions for the coefficients  $K_1$ ,  $K_2$  and  $T^*$  of the Shea and Moore (2010)  
 892 method. CMBC = S&M study area; AVDM = our study area. Outliers due to under-sampling at  
 893 freezing temperatures have been removed (as in the S&M work).  $\beta_3$  to  $\beta_7$  are coefficients from  
 894 S&M (J. M. Shea, personal communication), while the transfer function and coefficients for  $T^*$  are  
 895 new results from the present work.



896

897 Figure 7 - On-glacier temperature calculated with the Shea and Moore (2010) method vs. observed  
 898 temperature.

899

900

901

902

903

904

905

906

907

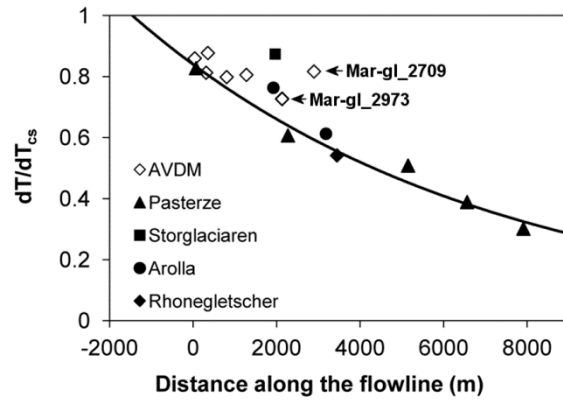
908

909

910

911

912



913

914 Figure 8 - Sensitivity of on-glacier temperature to temperature outside the thermal influence of  
 915 glaciers and best fit of Eq. (13) to Pasterze data. Redrawn figure from Greuell and Böhm (1998).  
 916 Values measured on Careser and La Mare glaciers (AVDM) have been added for comparison. Mar-  
 917 gl\_2973: two overlapping points (summer 2010 and 2011 have identical sensitivity).

918

919

920

921

922

923

924

925

926

927

928

929

930

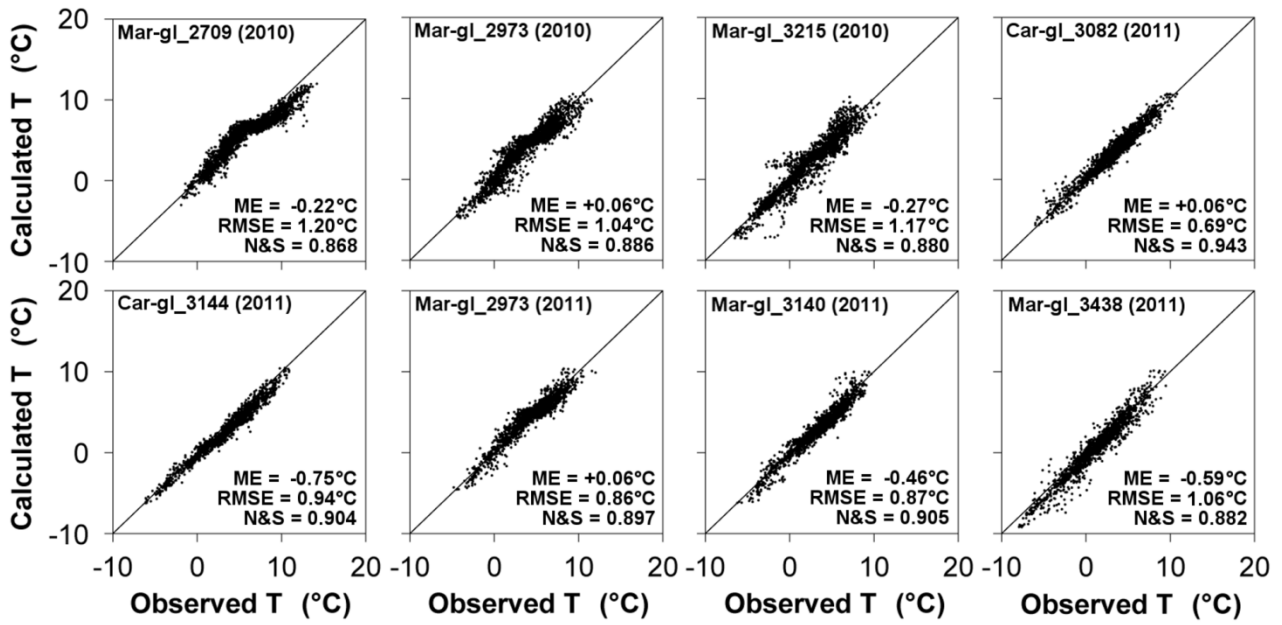
931

932

933

934

935

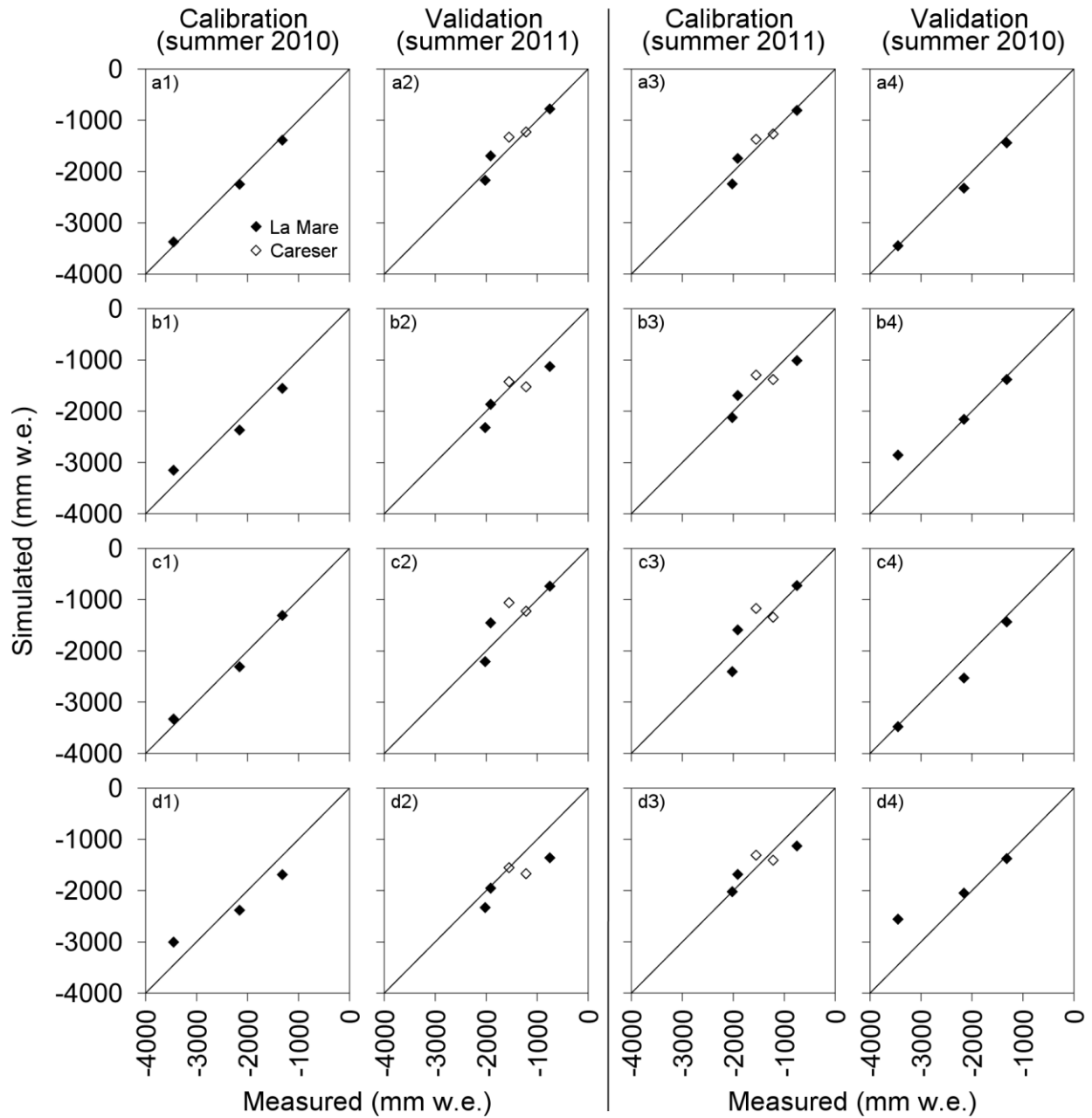


936

937

Figure 9 - On-glacier temperature calculated with the G&B method vs. observed temperature.





938

939 Figure 10 - Measured vs. modeled mass balance at the eight glacial weather stations, using  
 940 EISModel with four different air temperature inputs: a1 to a4 = measured; b1 to b4 = extrapolated  
 941 from Car\_2607 via the standard lapse rate ( $-6.5^{\circ}\text{C km}^{-1}$ ); c1 to c4 = calculated via the G&B method;  
 942 d1 to d4 = calculated via the S&M method. Corresponding statistics are reported in Table 6.